Journal of Energy Storage 30 (2020) 101422

Contents lists available at ScienceDirect

Journal of Energy Storage

journal homepage: www.elsevier.com/locate/est

Thermal kinetics on exothermic reactions of a commercial $LiCoO_2$ 18650 lithium-ion battery and its components used in electric vehicles: A review

Yih-Shing Duh[a,*], Xinzhong Liu[a], Xuepeng Jiang[b], Chen-Shan Kao[c], Lingzhu Gong[a], Ronghui Shi[a]

[a] Institute of Chemical Safety, Indoor Environment Engineering Research Center of Fujian Province, College of Ecological Environment and Urban Construction, Fujian University of Technology, Fuzhou, Fujian, China.

[b] Industrial Safety Engineering Technology, Research Center of Hubei Province, School of Resource and Environmental Engineering, Wuhan University of Science and Technology, Wuhan, Hubei, 430081, China.

[c] Department of Safety, Health and Environmental Engineering, National United University, Miaoli, Taiwan, ROC

ARTICLE INFO

Keywords:
Lithium-ion battery
Cathode material
Thermal kinetics
Thermal runaway
Calorimetry

ABSTRACT

A review gathering available results on the chemical kinetics in literature for the commercial 18650 lithium-ion batteries containing cathode material of $LiCoO_2$ and related components is summarized and discussed. Most of these kinetic parameters derived from adiabatic and heat-flow calorimeter, some few of them with the fitting of electrochemical-thermal model associated with data of accelerating rate calorimeter. However, due to the complexity of solid-state reaction involving both anode and cathode as well as the difficulty to determine the reaction mechanism function by thermal analysis on the solid electrode, most of the interpretation of calorimetric data set the order to be unity for simplicity. Kinetics-based heat rates under thermal abuses encompass the decomposition of solid electrolyte interface (stage III from 85 to 120 °C), reaction of Li_xC_6 with electrolyte (stage IV from 120 to 170 °C), reaction of Li_xCoO_2 with electrolyte (stage V from 170 to 200 °C), decomposition of Li_xCoO_2 (stage VI > 200 °C), decomposition of solvent (stage VI > 200 °C) induced by internal short, and auto-ignition of solvent (stage VI > 200 °C). To clearly capture the distinctive features of these kinetic behaviors, the standard deviations adopted by the American Society for Testing and Materials E2781 and International Confederation for Thermal Analysis and Calorimetry are applied to enhance the accuracy and precision of the kinetic parameters. A diagram integrating all the E_a and log A values of $LiCoO_2$ battery and its components is depicted, in which a newly phenomenon of compensation effect has been discovered. The linear equation of log A versus E_a tells the truth that some large errors existed in the data acquisition of kinetic parameters. Taking and comparing individually the average kinetic parameters from the decomposition of SEI, reaction of Li_xC_6 with electrolyte, reaction of Li_xCoO_2 with electrolyte to the whole battery, it is noteworthy that the chemical kinetics of the $LiCoO_2$ battery is next door to that of Li_xCoO_2 with electrolyte in n-th order reactions. The autocatalytic model II in E_a versus log A diagram seems to have the biggest deviations. The paradoxical model between the n-th order and autocatalytic type regarding the reaction of Li_xCoO_2 with electrolyte exists and has not been exactly solved. Practically, some unimaginable disagreement among parameters of E_a and log$A$ (sec^{-1} M^{1-n}) are as yet unsettled, which reveals that the more extensive studies are needed to resolve the existing disputes. For the near future, a breakthrough of exceedingly better technology for acquiring the accurate chemical kinetics of a $LiCoO_2$ battery and its ingredients will be expected earnestly.

Abbreviation: AKTS, Advanced Kinetics and Technology Solutions; ARC, Accelerating rate calorimeter; ASTM, American Society for Testing and Materials; CHETAH, Chemical Thermodynamic and Energy Release Program; CID, Current interrupt device; CISP, ChemInform Saint-Petersburg; DEC, Diethyl carbonate; DSC, Differential scanning calorimeter; DTA, Differential thermal analyzer; EC, Ethylene carbonate; EMC, Ethyl methyl carbonate; ESC, External short circuit; EV, Electric vehicle; EVARC, Extended volume accelerating rate calorimeter; HEV, Hybrid electric vehicle; HPLIB, Hard prismatic lithium-ion battery; ICTAC, International Confederation for Thermal Analysis and Calorimetry; ISC, Internal short circuit; LIB, Lithium-ion battery; MCMB, Mesocarbon microbead; OCV, Open circuit voltage; PC, Propylene carbonate; PE, Polyethylene; PP, Polypropylene; PTCD, Positive temperature coefficient device; RSST, Reactive system screening tool; SEI, Solid electrolyte interface; SOC, State of charge; STOBA, Self-terminated oligomers with hyper-branched architecture; TGA-MS, Thermogravimetric analyzer coupled with mass spectrometer; TPD-MS, Temperature-programmed desorption mass spectrometry; TST, Transition-state theory; VSP, Vent sizing package; XRD, X-ray diffraction

* Corresponding author.
E-mail address: yihshingduh@fjut.edu.cn (Y.-S. Duh).

https://doi.org/10.1016/j.est.2020.101422
Received 2 January 2020; Received in revised form 28 February 2020; Accepted 31 March 2020
Available online 29 April 2020
2352-152X/

Nomenclature

A, A_{01}, A_{02}	Frequency factor ($sec^{-1}M^{1-n}$)
C_0	Initial concentration of reactant (M)
C_p	Specific heat capacity ($Jkg^{-1}K^{-1}$)
E_a, E_{a1}, E_{a2}	Activation energy ($kJmol^{-1}$)
h	Planck constant (Jsec)
i	Electrical current (A)
k	Boltzmann constant (JK^{-1})
k, k_1, k_2	Rate constant (sec^{-1} M^{1-n})
k^*	Pseudo zero-order rate constant (sec^{-1} M^{1-n})
m,n,p	Order of reaction (dimensionless)
Q	Heat rate (Wm^{-3})
Q_{abuse}	Heat rate of abusive conditions in lithium-ion battery (Wm^{-3})
Q_{comb}	Heat generation rate from combustion reaction of electrolyte (Wm^{-3})
$Q_{dissipated}$	Heat dissipation rate (Wm^{-3})
Q_{ele}	Heat generation rate from decomposition of electrolyte (Wm^{-3})
$Q_{ele\text{-}chem}$	Heat generation rate from electrical-chemical reaction conversion (Wm^{-3})
$Q_{eletrical\ failure}$	Heat generation rate of electrical failure (Wm^{-3})
Q_{esc}	Heat generation rate of external short circuit (Wm^{-3})
$Q_{generated}$	Heat generation rate (Wm^{-3})
$Q_{irreversible}$	Heat generation rate of irreversible process (Wm^{-3})
Q_{isc}	Heat generation rate of internal short circuit (Wm^{-3})
Q_{ne}	Heat generation rate from reaction of lithiated anode material with electrolyte (Wm^{-3})
$Q_{overcharge}$	Heat generation rate of overcharge (Wm^{-3})
Q_{pe}	Heat generation rate from reaction of delithiated cathode material with electrolyte (Wm^{-3})
$Q_{reversible}$	Heat generation of reversible process (Wm^{-3})
$Q_{safety\ device}$	Heat removal rate by safety device (Wm^{-3})
Q_{sei}	Heat generation rate from SEI decomposition (Wm^{-3})
R	Universal gas constant (8.314 $Jmol^{-1}K^{-1}$)
T	Temperature (°C or K)
T_{amb}	Ambient temperature (°C or K)
T_{ave}	Average temperature of the lithium-ion battery (°C or K)
T_{cr}	Crucial temperature of lithium-ion battery under thermal runaway (°C or K)
T_{max}	Maximum temperature of lithium-ion battery under thermal runaway (°C or K)
$T_{max\text{-}rate}$	Temperature with the maximum self-heat rate (°C or K)
U	Open circuit voltage (V)
V	Equilibrium potential of battery (V)
ΔH	Enthalpy change ($kJmol^{-1}$)
ΔH_1	Heat of reaction for the formation of stable SEI from metastable SEI ($kJmol^{-1}$)
ΔH_2	Heat of intercalated lithium diffused from Li_xC_6 through SEI to react with EC ($kJmol^{-1}$)
$\Delta H^{0\neq}$	Enthalpy of activation ($Jmol^{-1}$)
$\Delta S^{0\neq}$	Entropy of activation ($Jmol^{-1}K^{-1}$)
ΔT	Adiabatic temperature rise (°C or K)
$<v>_{rel}$	Relative velocity of collision ($msec^{-1}$)
(dT/dt)	Self-heat rate ($°Cmin^{-1}$)
$(dT/dt)_{max}$	Maximum self-heat rate ($°Cmin^{-1}$)
x_f	Amount of metastable SEI (dimensionless)
x_i	Amount of intercalated lithium (dimensionless)
z_0	Initial amount of lithium in the SEI per unit surface area (m^{-2})
z	Amount of lithium in the SEI per unit surface area (m^{-2})

Greek and Latin

α	Degree of conversion (dimensionless)
α_0	Degree of conversion (dimensionless)
β	Parameter of autocatalytic reaction (dimensionless)
ε	Emissivity of the battery surface (dimensionless)
κ	Thermal diffusivity (m^2 s^{-1})
λ	Thermal conductivity ($Wm^{-1}K^{-1}$)
ρ	Density (kgm^{-3})
Ω	Reaction cross section of elementary reaction (m^2)
σ	Electrical conductivity of lithium ion in the electrode (Sm^{-1})

Subscript

cr	Crucial
max	Maximum
max-rate	Maximum-rate

1. Introduction

Since the first safety test on lithium-ion battery (LIB) by Yoshino in 1986 [1], the battery passed the iron lump test without ignition, it was the so-called time of the birth for lithium-ion battery. After further improvements SONY Corporation pushed lithium-ion battery into the commercialized generation. Lithium-ion batteries have been worldwide spread due to their features in high energy density, high power density, long cycle life, high electromotive force, thus with thin size, and low capacity loss during the time of storage, standby and normal operation. However, it holds dual characters within the battery itself, which has merits mentioned above in one hand associated demerits in another hand. Lithium-ion battery is prone to some abuses such high temperature environment, shock and vibration, mechanical crush, external penetration, overcharge and overdischarge, internal and external discharge, as well as external fire. These abusive scenarios can cause chemical affinity or electrical latent enthalpy transformed into heat generation leading temperature rise and even provoke the onset point of thermal runaway of the battery. Once the liberated heat cannot be dissipated by convection and radiation, thermal runaway of the problematic battery may be inevitable, which results in rupture, release, catch fire or explosion and so on. These are the reasons why the diverse lithium-ion batteries are considered to have the safety concerns, especially in large scale applications such as power sources of hybrid electric vehicles (HEVs), electric vehicles (EVs), and energy storage systems used for enterprise or houses. Even though $LiCoO_2$ batteries possess advantages and disadvantages, at present, the Tesla Roadster and Daimler Smart Fortwo are powered by $LiCoO_2$ batteries [2]. In order to avoid these abusive threatens, the safety mechanisms have been proposed to be equipped with these safety designs in a lithium-ion battery [3]. Strategies and designs for stopping or hindering the triggers of thermal runaway are developed and suggested using relief vent for overpressure, thermal fuse, circuit breaker, current interrupt device (CID), positive temperature coefficient device (PTCD) of ceramic or conductive-polymer types, shutdown separator, non-flammable solvent, redox shuttle, ionic liquid, and shutdown additive (such as self-terminated oligomers with hyper-branched architecture (STOBA)) [4,5]. Nevertheless, owing to the different electrode materials, electrolytes, salts, separators, exothermic chemistry, structures of internal layout, space, the processes of manufactures, much a few accidents or even major incidents have been occurred from time to time [6]. The well-known incident is the fire and explosion happened in the hard prismatic lithium-ion battery (HPLIB) of SAMSUNG Note 7 [7-10].

A variety of the thermal kinetics and exothermic behaviors of either

the batteries or relative components have been conducted by diverse calorimetry such as accelerating rate calorimeter (ARC) [11–15], vent sizing package (VSP) [16,17], reactive system screening tool (RSST) [18], differential scanning calorimeter (DSC) [19], temperature-programmed desorption mass spectrometry (TPD-MS) [20], C-80 microcalorimeter [21,22], copper slug calorimeter [23], cone calorimeter [24] and confinement set-up [10]. These calorimetry and spectrometry have been successfully applied in evaluating the thermal runaway consequences and exothermic characteristics of labile components for commercial or academic purposes. As the pioneers in battery safety-related development, the researchers in Dahn's laboratory verified the activation energy and frequency factor of exothermic reactions within battery's constituents using the DSC and ARC calorimetry [11–14]. For simplicity, reaction order was assumed to be the first order for both solid electrolyte interface (SEI) decomposition and the reaction of Li_xC_6 with electrolyte. Besides, kinetic models using Arrhenius type for the reaction of SEI film decomposition and that between lithiated graphite and electrolyte have been established [11,12]. In somewhat different feature for the reaction of Li_xCoO_2 with electrolyte, two different autocatalytic decomposition reactions were modelled [13,14]. Hatchard et al. built first the lumped thermal model based on the Biot number much less than 1 for cylindrical and prismatic lithium-ion batteries [25]. In Hatchard's model only three exothermic reactions of the SEI decomposition, Li_xC_6 with electrolyte and an auto-catalytic model below 200 °C for the $LiCoO_2$ with electrolyte were presented. Spotnitz and Franklin extended the similar model to more electrode materials and electrolytes except $LiCoO_2$, in their plentiful study, a set of E_a and log A of electrolyte decomposition was first reported [26]. Kim et al. [27] further applied the 1D to 3D simulation, a main frame of thermal model was built by adding the fourth term of the exothermic decomposition of electrolyte. A thermal abuse model was modified to analyze the thermal runaway behaviors of lithium-ion batteries which were validated against experimental results for conventional oven tests by Lopez et al. [28]. Recently, delicate modification or improvement in the considerations of diverse cathode materials by Peng and Jiang [29], venting and ejecta by Coman et al. [30], critical parameters by Melcher et al. [31], safety-focused model by Abada et al. [32], runaway-induced deflagration by Ping et al. [33], model-based thermal runaway by Ren et al. [34], internal short circuit (ISC) to thermal runaway model by Feng et al. [35], external short circuit (ESC) to thermal runaway model by Lee et al. [36], overcharge to thermal runaway model by Ren et al. [37], state of charge (SOC) and the charge/discharge processes on the thermal runaway of lithium-ion batteries [38,39], runaway mechanisms of lithium-ion batteries based on thermal analysis database [40] and so on, the coupled electrochemical-thermal models [41] have reached the acme of perfection. Most of the parameters used in these thermal models, especially the common $LiCoO_2$/graphite chemical kinetics followed the steps of Dahn's study and Hachard's model for near 20 years.

Some more innovative studies breaking through the bottleneck of the joint between safety issues and chemical kinetics have been implemented. The chemical kinetics with regards to $LiNi_xMn_yCo_zO_2$(NMC) chemistry in the study of Ren et al. and $LiNi_{0.8}Co_{0.15}Al_{0.05}O_2$(NCA) chemistry in the work of Lee et al. have been respectively determined by DSC and ARC using Kissinger's methodology and fitting in thermal curves [34,36]. Energetics of commercial lithium-ion batteries were measured by bomb calorimetry or fire calorimetry [33,42]. Spotnitz and Franklin have summarized the detailed stages and mechanisms of thermal abuse to trigger the thermal runaway of a lithium-ion battery in relation to temperature [26]. In a similar way, another five stage model with specific temperature regions was suggested by Feng et al. for thermal runaway of large format prismatic lithium-ion battery using extended volume accelerating rate calorimeter (EVARC) [43]. Soon after the notification, Duh et al. proposed the six stage model by correlating the self-heat rate with temperature on thermal runaway of commercial hard prismatic lithium-ion batteries used in smart phones [10]. Diverse stages of the progression and propagation of thermal runaway were suggested according to the temperature, overcharge status or material analysis after thermal runaway were argued [15,33,43,44]. A newly time sequences of thermal runaway with different characters and thermal runaway of commercial with internal short circuit hold a lead to declare the mechanical phenomena of the thermal runaway inside lithium-ion batteries [45]. In conjunction with the thermal runaway kinetics of $LiCoO_2$ battery, a set of rate equations for oxygen evolution by decomposition of Li_xCoO_2 at elevated temperatures using the thermogravimetric analyzer coupled with a mass spectrometer (TGA-MS) was proposed by Yamaki [46]. Further information on the microscopic viewpoint on decomposition, a phase-field modeling study oxygen evolution and phase transformation in Li_xCoO_2 cathode was depicted by Yurkiv et al. [47].

Despite the importance and requirement of chemical kinetics on exothermic behavior in relation to lithium-ion battery and its components, even this day, the accurate and precise kinetic parameters regarding the runaway stages have never assured. There exists a large discrepancy or a gap in the kinetic triples (reaction model, frequency factor and activation energy) between laboratory or within the laboratory, even though the delicate calorimeters were used in acquiring experimental data with further treatment of commercial software based on famous kinetic models. The reaction model is well-accepted as $f(\alpha)$, representing a number of physical transformations and chemical reactions, which has been worldwide applied in solid-state reactions and related fields [13,14,48,49]. Some large deviations occurred between laboratory and within laboratory can be seen as follows: For example, by the uses of kinetic data regarding cathode materials of $LiCoO_2$, $LiNi_{0.8}Co_{0.15}Al_{0.05}O_2$, $Li_{1.1}Ni_{1/3}Mn_{1/3}Co_{1/3}CO_2$, $LiFePO_4$, and $LiMn_2O_4$ the onset temperature were calculated to be 175, 200, 255, 260 and 270 °C [29], which did not agree with the onset temperature of commercial 18650 batteries determined by various calorimetry [50-55]. In addition, several attempts have focused on the thermal runaway of commercial 18650 batteries induced by internal short circuit, some disputes regarding the maximum temperature and maximum self-heat rate differed each other and did coincide with the results studied by calorimetry. For $LiCoO_2$ 18650 batteries with the common cathode material , the maximum temperatures were quite different from simulations such as 250 °C (surface temperature at 155 °C oven temperature) [27], 350 °C (surface temperature [28]), 760 °C (surface temperature) [56] and 1150 °C (core temperature) [57]. However, the maximum temperatures were experimentally determined in the range from 340 °C to 903 °C by adiabatic calorimetry [16,55,58]. Especially to deserve to be mentioned, the maximum self-heat rate spanned from 640 to approximately 10000 or 77286 °C min^{-1} which were detected by various calorimeters [16,55,58]. Obviously, the biased quantities of these maximum temperature and maximum self-heat rate in the published literature are too huge to be convincing so far forth. These conflicts and errors arouse from the inaccurate chemical kinetics of $LiCoO_2$ battery. This is lucid and easy to understand that the Arrhenius parameters decide the outcomes by simulation and the fates of thermal runaway of the lithium-ion batteries under thermal abuses are the representations of the kinetic parameters possessed within the batteries. Practically, such large deviations cannot be seized of precise applications by kinetics, nor can offer useful guidance in designing a better battery.

Due to most of the thermal models in the literature are based on the world-famous model developed by Hatchard et al. [25] and kinetic triplet from calorimetric data from Dahn and his coworkers [11-14]. It is worthy of gathering the chemical kinetics of $LiCoO_2$ battery and its components, all together to reassess the accuracy and precision of reported kinetics. Unfortunately, in the two decade this work has not been accomplished. The first objective of this study is to integrate the published kinetic parameters in regard to the decomposition of SEI, the reaction of lithiated carbonaceous material (Li_xC_6) with electrolyte, decomposition of Li_xCoO_2, reaction of Li_xCoO_2 with electrolyte, and decomposition of electrolyte in relation to the lumped kinetics of a

whole lithium-ion battery. The second is, the treatment using standard deviations by the recommendations of the American Society for Testing and Materials (ASTM) E 2781 [59] and the International Confederation for Thermal Analysis and Calorimetry (ICTAC) [60] in filtering noise or fluctuation of kinetic data, to get the reliable kinetics. In the light of accurate data, the authors would like to propose the new idea of "kinetics window" of the $LiCoO_2$/graphite battery. For the third objective, it is worth justifying which component is the most crucial part to decide the destiny of the chemical kinetics for a whole $LiCoO_2$ battery. This work is eager to know the autocatalytic model of Li_xCoO_2 reacted with electrolyte have been applied in thermal model about 10 times, however, the autocatalytic model has not been announced in an unit battery. Based on emphasizing the above-mentioned reasons and to solve the kinetic triplet in the long term, the fourth objective for declaring the drastic variation and gigantic differences in kinetic parameters is ardently expected to be executed later on. Besides, is there any possibility that the compensation effect will be occurred in an E_a versus log A diagram or not. Once acquiring the accurate and precise kinetic triplet associated with the thermo-analytical methodology in the components and the lithium-ion battery itself, perhaps, these prerequisites can point the hopeful direction to the future designs of inherently safer batteries in the next generation. The last objective of this work is to try to figure out an effective practice from calorimetry and thermal analysis related to the solid-state reaction for evaluating accurately and precisely the kinetic parameters.

2. Lithium-ion battery Systems

2.1. Physical system and structure

A commercial lithium-ion battery with the discrete structures generally contains hundreds of unit cells in the form of concentric spirals [26]. These spirals, being the major frame and structure of jellyroll, were compelled to a consolidated and tight space inside the cell. Flat but thin sheets of metals (for example, Ni and Cu) comprising the anode, electrolyte, separator and cathode of the cell are stacked one on the other rolling very tightly together like a jellyroll. The tight roll of unit cells is then congested into a metal cylinder from an open top, then eventually capped and sealed leaving the positive pole upward. For simplicity, a unit cell is modelled as a slab consisting of layers of composites made of anode, cathode, electrolyte, separator and binder. The internal structure of the battery is actually considered as discrete, which the active material is made from smaller regions defined by each layer inside the unit cell and its specific physical and chemical properties.

2.2. Energy equation under normal operation

After Bernardi et al. [61] declared the first thermal model for an electrochemical cell, Newman with his colleagues reconstructed and simplified the energy equation [62,63]. The Bernardi-Newman theory was built on an electrochemical description of diffusion dynamics, charge transfer kinetics and thermodynamics of a battery which can predict the thermal or electrical response of a rocking chair battery [61-63]. This has been called as an electrochemical-thermal modeling, which coupled of electrochemical kinetics, charge conservation, mass transport and heat transfer to construct the thermal model within the battery. The energy equation can integrate the above-mentioned effects to predict the temperature distribution in a battery. There are three heat sources considered in the analysis of thermal runaway under the normal operation temperature is generally between -40 to 60 °C. The expression integrating the heat generated by electrochemical charge/discharge reactions, Joule and Ohmic effects as well as reversible and irreversible enthalpy changes can be written as follows:

$$\frac{dQ}{dt} = \rho C_p \frac{\partial T}{\partial t} = Q_{generated} - Q_{dissipated} \tag{1}$$

$$Q_{generated} = Q_{irreversible} + Q_{reversible} + Q_{mixing} = i(U - V) - iT\left(\frac{\partial U}{\partial T}\right)_p + Q_{mixing} \tag{2}$$

where dQ/dt is the heat rate of the battery; ρ is the density, C_p is the heat capacity and T is the temperature of battery; $Q_{generated}$ is the heat generation rate during battery operation containing ion transport, electrochemical reaction and charge/discharge processes; $Q_{irreversible}$ is the heat rate of irreversible process from over-potential or polarization effect; $Q_{reversible}$ is the heat rate of reversible process from electrochemical reaction; i is the electric current; U is the open circuit voltage; V is the battery equilibrium voltage; $(\partial U/\partial T)_p$ is the temperature coefficient of U; Q_{mixing} is the heat rate from the concentration gradients in migrating ion and electrolyte; $Q_{dissipated}$ is the heat flow rate of dissipation by conduction from the cell passing the boundaries of battery to the reservoirs. The rate of environmental convection transfer can be expressed as $h(T\text{-}T_{amb})$ where h, and T_{amb} are the convective transfer coefficient and ambient temperature, respectively. By obeying the theory of black-body radiation, the rate of radiation transfer depends on the fourth power of the surface temperature, $\varepsilon\sigma(T^4\text{-}T_{amb}{}^4)$, in which σ is the Stefan-Boltzmann constant and ε is the emissivity of the battery body. At the boundaries, both the heat transfer by convection and radiation have to be included in all. Thus, heat rate of dissipation can be further expressed as:

$$Q_{dissipated} = \nabla(\kappa \nabla T) = h(T - T_{amb}) + \varepsilon\sigma(T^4 - T_{amb}^4) \tag{3}$$

2.3. Energy equation with electrical failures

To explore the thermal runaway of 18650 battery microscopically, the initiation and propagation of thermal runaway have been proved by high-speed tomography and by internal discharge using direct short between Al of cathode and graphite of anode [64,65]. Finegan et al. posed the evolution of the internal structural damage and thermal behavior during initiation and propagation of thermal runaway of a commercial 18650 NMC battery using the high-speed tomography and radiography associated with thermal imaging [64]. By heating the battery using a heat gun, the authors found that thermal runaway can lead to the collapse of the electrode and structure, and also melting of current-collecting materials. Analyzing the ISC is a challenging task being tackled by more and more authors [66-67]. Some focused on experimental studies on different types of cells, but only a few studies have been performed in modeling the ISC. By combining modeling and experimental validations, both Santhanagopalan et al. [65] and Feng et al. [35] showed that the short circuit between the aluminum current collector and the negative electrode produced the highest subsequent heat generation, and led to the maximum local temperature inside the battery. Some other significant modeling efforts on the different internal short-circuit scenarios that can occur between different cell components were performed and reviewed by Feng et al. [35]. Using a three-dimensional electrochemical-thermal model coupled with the electrical abuse, the correlation between the measured data of voltage, resistance, and temperature with the abusive status was established. Especially, Santhanagopalan et al. assessed the severity of the electrode material under short-circuit contact [65]. Lee et al. developed a thermal-runaway model of lithium-ion battery by contriving a resistive heating from an external short circuit with the well-known electrochemical-thermal conversion of lithium-ion battery [36]. An overcharge test was first simulated by Spotnitz and Franklin [26] who introduced overcharge in their model by adding the following specific generation rate term, $Q_{overcharge}$, to the cellular energy equation. Simulations of overcharge conditions with this model showed that the subsequent thermal runaway was mainly driven by metallic lithium

reacting with the solvent in the cell. Ren et al. inaugurated a model of electrochemical-thermal coupled with overcharge to predict the electrochemical and thermal responses of lithium-ion battery [37]. Conceptually, the above-mentioned heat rate related to electrical abuses is basically derived from the Ohm's law. To adopt the electrical abuses, extensive modeling efforts in dealing with triggering events such as internal or external short-circuits, overcharge, and overdischarge have been explored with controlled conditions. Under these circumstances to simulate thermal runaway triggered by electrical failures, equation (2) can be modified by equation (4) then rewritten as equation (5) for such purposes:

$$Q_{generated} = Q_{electrical\ failure} = Q_{ISC} + Q_{ESC} + Q_{overch\ arg\ e} \tag{4}$$

$$Q_{generated} = i(U - V) - iT\left(\frac{\partial U}{\partial T}\right)_P + Q_{electrical\ failure} \tag{5}$$

2.4. Energy equation with thermal abuses

A considerable endeavor of model for the thermal responses under credible abuses of both cylindrical and prismatic lithium-ion batteries has been widely made. Several simulated works have been accomplished to validate the matching of thermal kinetics and mathematical models for the thermal responses of both 18650 and prismatic lithium-ion batteries. For cylindrical ones, thermal models can be defined in zero, one, two and three dimensions. The zero dimension is also termed as a “lumped” model. To do this simply, the discrete unit cells are often to be treated as a homogeneous state, that is, the active material is considered as a single phase weighted from the whole physical and chemical properties of each layer inside the battery. It is desirable from the theoretical point of view, abuse behaviors are simulated by setting the internal heat generation rate of the cell to a high value for a short time and to accompany the temperature profile propagating with time, which indicated that the thermal runaway could simulate real events of an internal short circuit or exothermic side reactions. Exposure test at constant temperature in the oven or hot stage is a standardized test that the lithium-ion must pass and be certified for safety before sale by regulatory units. Using Arrhenius-typed reactions that have been developed for SEI decomposition, electrode material reaction with electrolyte, and physical properties of battery from the literature, a predictive model for oven exposure testing has been developed.

It is known to all, a thermal abuse system is defined as the lithium-ion battery under high temperature, such as external fire or hot surface which causes the temperature rise to surpass the onset temperature of exothermic reactions. Unless the extremely large electric current resulted from the charge and discharge with high capacity as well as the self-heat rate from electrochemical-thermal reaction are both comparable to those came from thermal abuses, the heat from electrical circuits and electrochemical lithiation or delithiation are temporarily overlook under the scope of thermal abuse. Actually, the lithium-ion batteries have been assumed under an adiabatic condition before and after the propagation of thermal runaway inside an accelerating rate calorimeter. Therefore, the energy equation can be simplified as:

$$\rho C_p \frac{\partial T}{\partial t} = Q_{generated} = Q_{thermal\ abuse} \tag{6}$$

An integrated equation to sum up the heat-releasing rates correlated with the exothermic reactions under thermal abuses has been widely known to date [25,27-29].

$$Q_{thermal\ abuse} = Q_{sei} + Q_{ne} + Q_{pe} + Q_{ele} \tag{7}$$

where Q_{sei} is the heat generation rate from SEI decomposition, Q_{ne} is the heat generation rate from reaction of Li_xC_6 with electrolyte, Q_{pe} is the heat generation rate from reaction of Li_xCoO_2 with electrolyte, and Q_{ele} is the heat generation rate from electrolyte decomposition.

2.5. Battery safety and design related to chemical kinetics

From design to commercialization stage of a lithium-ion battery, it suffers the so-called “design and test” as well as “trial and improvement” processes which are not only time-consuming and money-spending but also challenging. In order to test the chemistry, design, materials for performance and safety for a new type battery, engineers have to produce the pilot batches of batteries, say about 50 units. All the electrochemical performances and safety have to be optimized as far as possible. Safety problem occurred in lithium-ion battery is a complex phenomenon related in physics, chemistry, engineering, manufacture and economics. Design parameters may have an important engineering indication of a safe LIB design. Consequently, as an alternative way, using modeling and simulation to predict battery safety and performance, which the normal or abusive processes can be quantitatively and qualitatively assessed. By the roots, performance and safety issue of a battery is one integrity with both sides, which can be integrated together. In summary, a governing energy equation adding safety device is rewritten from the equations (1), (3), (4), and (7) as follows:

$$\rho C_p\left(\frac{\partial T}{\partial t}\right) = Q_{irreversible} + Q_{reversible} + Q_{electrical\ failure} + Q_{thermal\ abuse} - Q_{safety\ device} - Q_{dissipated} \tag{8}$$

It is critical that this electrochemical-thermal coupling model associates the kinetics term embedded in $Q_{thermal\ abuse}$ with the intentional engineering parameters to be studied. In which $Q_{irreversible}$ and $Q_{reversible}$ belong to the electrochemical reactions under normal operation within the temperature difference less than 20 °C. The cell size, shape, can, heat transfer materials and cooling design in battery pack are in relation to heat dissipation of $Q_{dissipated}$. $Q_{electrical\ abuse}$ takes into account of internal/external short circuit, overcharge and over-discharge. Hot spots produced from mechanical abuses such as nail penetration or crushing can be included in $Q_{thermal\ abuse}$. Chemical kinetics and exothermic reactions linked to anode/cathode chemistry, decomposition of SEI, reaction or decomposition of electrolyte, decomposition of anode or cathode and oven exposure can be merged into the $Q_{thermal\ abuse}$. Safety devices can act as quencher or thermal retarder by their current-limiting, current-interrupting, or resistance-increasing mechanisms for impeding the progressing of thermal runaway inside

Table 1
Chemical kinetics in relation to battery design and safety mechanism

Term in energy equation	Kinetic parameter/engineering parameter/safety device
$Q_{thermal\ abuse}$	E_a, A and n for Q_{sei}, Q_{ne}, Q_{pe} and Q_{ele}
$Q_{irreversible}$	electrical current, overpotential, mixing of concentration gradient, phase change
$Q_{reversible}$	entropic effect of $(\partial U/\partial T)_p$
$Q_{electrical\ abuse}$	Q_{isc}, Q_{esc}, overcharge current, SOC, open circuit voltage (OCV)
$Q_{safety\ device}$	thermal fuse, circuit breaker, shutdown separator, lithium salt, Redox shuttle, inhibitor for thermal runaway, safety vent, PTC, STOBA
$Q_{dissipated}$	size, diameter, ratio of radius to volume, heat transfer material of battery, cooling capacity, battery pack, thermal management system

Note: Action and operation temperature of safety devices: thermal fuse (90-110°C); STOBA (100-120°C); PTC(100-130°C); circuit breaker ($\Delta T/\Delta t$); shutdown separator PE (135°C); shutdown separator PP (165°C); safety vent (5-25 psig at set pressure or set temperature) [3-5, 68,69].

the batteries in case of abusive events. Therefore, the $Q_{\text{safety device}}$ is introduced in equation (8). Conventional safety devices include thermal fuse, STOBA, PTC, circuit breaker and shutdown separator made of polyethylene (PE) or polypropylene (PP) or their composites [3-5,68,69]. Moreover, some safety mechanisms have been designed to temper the exothermic reactions by redox shuttles, non-flammable solvents, runaway inhibitors, ionic liquids, lithium-ion salts, and safety vents [3]. Optimization the design data in acquiring a better or inherently safer battery is believed to be the state-of-the-art. Chemical kinetics reinforces itself in the equation (8) for the safer and newer design of the lithium-ion battery can be correlated in Table 1.

3. Calorimetry and Methodologies for acquiring kinetic parameters

3.1. Thermoanalytical methodology

From the thermoanalytical methodology regulated by the standards of ASTM[70-72], the non-isothermal curve detected from components of lithium-ion batteries must be a simple curve if the rate constant obey Arrhenius equation and with the intrinsic features of homogeneous reactions of n-th order. Thermoanalytical methodology (such as DTA, DSC and TGA) takes an aggregate and bulk signal of all elementary reactions occurring in the reactant. As experienced, this means that the exothermic curve must be a smoothly well-behaved one with nice conversion versus temperature relation. Perturbations of shoulders, overlapped multiple peaks, shifts in baselines or discontinuous steps have to be excluded in the qualified curves. The applications of this simplified model in the autocatalytic reaction, consecutive reaction, heterogeneous reaction, inhibited reaction, parallel reaction and solid-state reaction should be avoided and with the cautions notified by several standard methods of ASTM [70-72]. Kinetic parameters related to the thermal curve can be extracted by using a suitable kinetic model such as methods of Borchardt & Daniels [73], Friedman [74], Flynn/Wall/Ozawa [75-77] or Kissinger [78]. Most of all, a homogeneous system of Arrhenius type reaction and approximation of single-step kinetics are always adopted for determination of kinetic triplets. Approaches or software package for analyzing the kinetic parameters such as the method of Borchardt & Daniels (ASTM E2041) [70], method of Kissinger (ASTM E2890) [72], method of Flynn/Wall/Ozawa (ASTM E698) [71], software packages supplied by the Advanced Kinetics and Technology Solutions (AKTS) [79] and the ChemInform Saint-Petersburg (CISP) [80] have been universally executed.

3.2. Accelerating rate calorimeter (ARC) and Townsend's theory

In addition to the standards of thermal analysis regulated by ASTM and along with a better visualization, these kinetic parameters can be also assessed by the adiabatic calorimeters such as an ARC. By using the adiabatic thermal curve acquired from ARC, data analysis is based on the assumption of the simple reaction scheme proceeding by one reactant. In short, conversion of reaction extent defined by mass is simplified by the replacement of enthalpy conversion or temperature conversion associated with the chemical equation of A → P. By obeying the Townsend's theory in conjunction with the application of adiabatic calorimetry [81], kinetic parameters (reaction order, activation energy and frequency factor) on thermal runaway of a whole battery or its components can be deduced. Intrinsically, k is proportional to self-heat rate (dT/dt) in rate equation. By defining the pseudo rate constant k^* and via the method of trial and error, the Arrhenius-like plot of ln (k^*) as a function of the reciprocal of absolute temperature was used to identify the reaction order. A linear fitted line can thus be obtained by selecting a correct n in the front, thereon E_a (kJ mol^{-1}) and A (sec^{-1} M^{1-n}) will be explicitly expressed as a straight line of ln (dT/dt) vs. $1/T$ without the distorted nonlinear temperature dependence. For further understanding the detailed performance and applications of the ARC instrument which can be referred to the Townsend's theory [81] or ASTM E1981 [82].

Note: For simplicity, the unit sec^{-1} M^{1-n} will be expressed as sec^{-1}in the subsequent sections.

4. Results and Discussion

4.1. Thermoanalytical kinetics of decomposition of SEI

The formation process of SEI film on carbonaceous electrode during the initial cycle, which takes place at the narrow voltage range of 0.25-0.04 V vs. Li+/Li by the reaction of ethylene carbonate (EC) with Li^+ on the surface of anode [83]. This stage, which proceeds simultaneously with lithiation of graphite electrode to accompany a stable, compact, and highly conductive SEI film with an excellent electrochemical performance. The kinetic parameters on the thermal decomposition of SEI were first determined by Richard and Dahn using ARC and a specially designed thin tube with high sensitivity holding the thermal inertia near unity [11,12]. The reaction order was assumed to be first, the activation energy (E_a in kJmol^{-1}) and log A (frequency factor A in sec^{-1}) were determined to be 135.1 and 15.2, respectively [11,12]. After successive studies on the SEI decomposition of various carbonaceous materials, without a decision of reaction order and ignore the salt effect of $LiBF_4$, the E_a and log A with a respective average value of 139.8 kJmol^{-1} and 15.9 were proposed by MacNeil et al. [84]. Chen et al. reported a set of lower E_a ranged from 53 to 92 kJ mol^{-1} without any interpretation of frequency factor or reaction order [85]. Being took part in the parameterized thermal model, the similar E_a and log A in comparison to the data of Richard and Dahn were adopted by Coman [56]. Table 2 lists the kinetic parameters on the thermal decomposition of SEI [11,12,26,30,34,84,85]. Fig. 1 shows the relation of E_a versus log$A$ of the SEI decomposition. However, Spotnitz & Franklin got the extremity of the highest E_a among these kinetic data reported [26].

4.2. Thermoanalytical kinetics on intercalated graphite with electrolyte

A mysterious reaction that has a detectable signal is the exothermic reaction between intercalated graphite (Li_xC_6) and electrolyte. Richard and Dahn determined the respective E_a and log A (A in sec^{-1})to be 77.2 kJ and 6.2 using ARC as well as assuming the order of reaction to be unity for simplifying the self-heat equation[12]. Using ARC, Hatchard et al. took the n, E_a, and log A to be 1, 135.1 and 13.4, respectively [25]. Coman et al. [56] presented the thermal runaway under oven exposure by simulation and had the fitted E_a and log A being 134.8 kJmol^{-1}and 14.8. By using DSC, Yang et al. depicted the E_a between three reaction

Table 2
Kinetic parameters on thermal decomposition of SEI [11,12,26,30,34,84,85]

SEI	Calorimeter	Order (n)	E_a (kJ mol^{-1})	Log A (sec^{-1})	Reference
SEI	ARC	1	135.1	15.2	[11,12]
SEI	NA	NA	281.0	36.9	[26]
SEI	Fitted	NA	134.8	15.0	[30]
SEI	DSC	5.5	109.6	9.8	[34]
MCMB	ARC	NA	135.1	14.9	[84]
MCMB($LiBF_4$)	ARC	NA	79.1	8.9	[84]
SFG-75	ARC	NA	144.7	16.0	[84]
SFG-44	ARC	NA	144.7	16.4	[84]
KS-75	ARC	NA	125.4	14.5	[84]
XP3	ARC	NA	144.7	16.5	[84]
Fiber	ARC	NA	144.7	16.8	[84]
MCMB-1028	DSC	NA	53.0	NA	[85]
SMG-N-7b	DSC	NA	88.0	NA	[85]
SMG-N-20	DSC	NA	92.0	NA	[85]
SMG-Ns-15f	DSC	NA	78.0	NA	[85]

Note: NA, Not available; In reference 84 and 85, several product names of anode materials were given, such as mesocarbon microbead (MCMB).

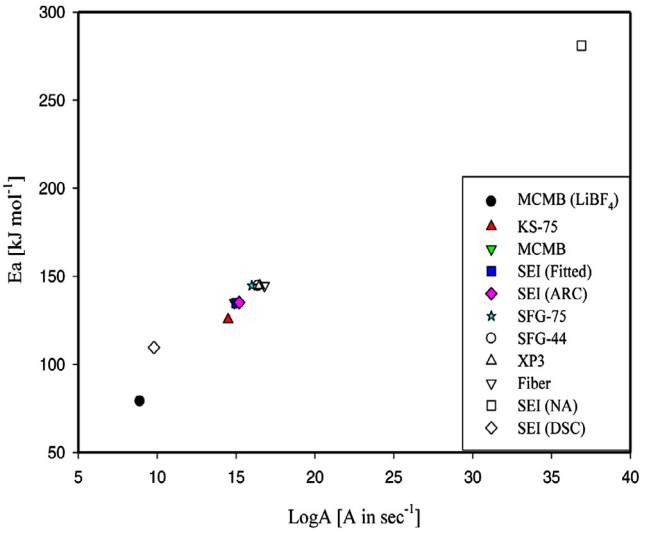

Fig. 1. Relation of activation energy versus log*A* of SEI decomposition

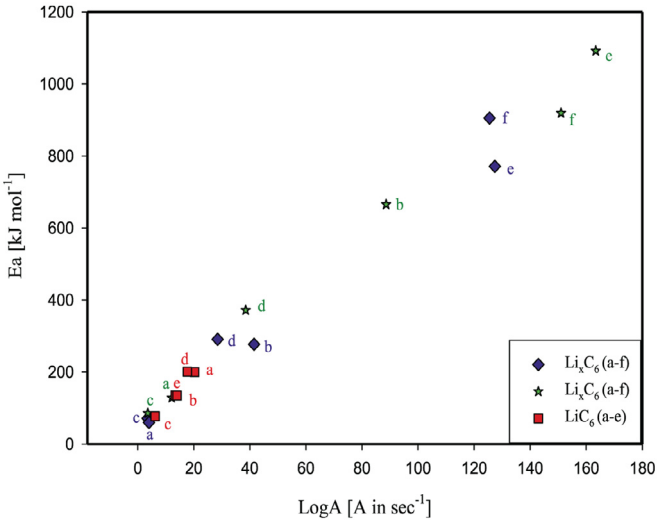

Fig. 2. Relation of activation energy versus log*A* regarding Li_xC_6 reacted with electrolyte

system of $Li_{0.71}C_6$ (Mag-10), $Li_{0.91}C_6$ (Mag-10), and $Li_{0.91}C_6$ (GDR) with electrolyte to be 137.0, 108.0 and 82.0 kJmol^{-1}, respectively [86]. However, Spotnitz and Franklin announced the highest E_a and log A among these literature's data [26]. For solving the complicated and overlapped thermal curve related to the reaction of LiC_6 with electrolyte, an unusual peak separation method was posed by Ping et al. [22] to deconvolute the lumped thermal curve into six single step reactions with its individual Arrhenius parameters. The kinetic parameters of the reaction of lithiated graphite with electrolyte are shown in Table 3 [12,22,25,26,34,56,86]. Fig. 2 depicts the relation of E_a versus log A. As can be seen from their kinetic data in Fig. 2, the Arrhenius parameters spanned a very wide range which can cause some provoked discussion.

4.3. Thermoanalytical kinetics of delithiated cathode materials with electrolytes

4.3.1. Kinetics of decomposition of $LiCoO_2$

Property of $LiCoO_2$ had been a hot focus of research and commercial interests, not only its electrochemical performance, but also the toxic property need to be improved or substituted. With an admirable consistency, the exothermic onset temperature of $LiCoO_2$ with electrolyte was also detected to be about or higher than 350 °C by DSC [87,88]. As known to all, the Li_xCoO_2 is extremely unstable in this delithiated state under the charging process in lithium-ion battery. MacNeil et al. and Baba et al. have concluded that the $Li_{0.5}CoO_2$ in delithiated state reacted with EC/DEC(diethyl carbonate) in a lower temperature than the decomposition of $Li_{0.5}CoO_2$ itself, accompanying oxygen generated from $Li_{0.5}CoO_2 \rightarrow LiCoO_2 + (1/6)\ Co_3O_4 + (1/6)\ O_2$ at temperature above 200 °C [89,90]. Thereafter, the catastrophic thermal runaways occurred in lithium-ion batteries above 200 °C have thus been deduced to be the oxidation reactions between the liberated oxygen and organic carbonates in electrolytes. In accordance with the above mentioned, temperature dependence of oxygen evolution was identified by using temperature programmed desorption-mass spectrometry [20]. Even the $LiCoO_2$ was heated to 600 °C, oxygen was not generated. On the other hand, delithiated Li_xCoO_2 liberated oxygen above 250 °C [89]. Furushima et al. employed a nonisothermal kinetic analysis using the model free iso-conversional method (Friedman-Ozawa plot) to estimate the activation energy of decomposition Li_xCoO_2 [20]. From the plot of $\ln(d\alpha/dt)$ versus $1/T$, several straight lines with a constant slope between the conversions from 5 to 70% were obtained. A slope of $(-E_a/RT)$

Table 3
Kinetic parameters on reaction of lithiated graphite with electrolyte [12,22,25,26,34,56,86]

Anode Material	Electrolyte	Calorimeter	Order (n)	E_a (kJ mol^{-1})	Log A (sec^{-1})	Reference
LiC_6	NA	ARC	1	77.2	6.2	[12]
Li_xC_6	1.0MLiPF$_6$/EC + DEC(1:2.2)	C-80	NA	a:59.7	a:4.0	[22]
				b:277.0	b:41.5	
				c:71.2	c:3.5	
				d:290.9	d:28.5	
				e:771.2	e:127.4	
				f:905.0	f:125.5	
Li_xC_6	1.0MLiPF$_6$/EC + DEC(1:1)	C-80	NA	a:128.6	a:12.1	[22]
				b:665.4	b:88.6	
				c:85.5	c:3.6	
				d:371.7	d:38.5	
				e:1091.7	e:163.4	
				f:919.1	f:151.0	
LiC_6	NA	ARC	1	135.1	13.4	[25]
LiC_6	NA	NA	NA	200.0	20.3	[26]
Li_xC_6	1.0MLiPF$_6$/EC + DEC + DMC (1:1:1)	DSC	1	200.8	17.7	[34]
LiC_6	NA	Fitted	NA	134.8	14.0	[56]
$Li_{0.71}C_6$ (Mag-10)	NA	DSC	NA	137.0	NA	[86]
$Li_{0.91}C_6$ (Mag-10)	NA	DSC	NA	108.0	NA	[86]
$Li_{0.91}C_6$ (GDR)	NA	DSC	NA	82.0	NA	[86]

Note: NA, Not available

and E_a can be obtained by plotting the ln(dα/dt) against 1/T within a linear range. The authors reported that an average value E_a of $Li_{0.81}CoO_2$ and $Li_{0.65}CoO_2$ determined to be 130 and 97 kJ mol^{-1}, respectively. However, Wang et al. [91] argued that the activation energy of $LiCoO_2$ charged to 4.2 V was 148.9 kJ mol^{-1} from TGA, and a lower value of 88.9 kJ mol^{-1} from C-80 calorimeter using the method of Borchardt & Daniels. Table 4 displays the kinetic parameters determined by various analytical techniques [20, 30, 91]. Due to lack of the data log$A$, the relation of E_a versus log$A$ in neat Li_xCoO_2 decomposition can not be presented in a Figure.

4.3.2. Thermoanalytical kinetics of reaction of delithiated cathode materials with electrolytes

Delithiated $LiCoO_2$ occupies the majority of cathode materials reacted with electrolyte due to the importance described in the above section. MaceNeil et al. first tried to figure out the thermoanalytical behavior of the reaction between Li_xCoO_2 and electrolyte [13,14]. A solid-state reaction with an autocatalytic model was established to simulate the thermal curve of ARC and DSC [13,14]. Two set data were reported with the (E_a, log A) to be (123.9 kJ mol^{-1}, 11.4) and (153.4 kJ mol^{-1},14.5) [13,14], respectively. In an attempt to account for their results of simulations on the thermal runaway of a $LiCoO_2$ battery, several research groups arrived at the quite close results of Arrhenius parameters as follows: the E_a and log A to be 122.5 and 11.8 by Hatchard et al. [25]; the E_a and log A to be 139.6 and 13.8 by Kim et al. [27]; the E_a and log A to be 122.5 and 11.8 by Peng et al. [29]; the E_a and log A to be 122.2 and 13.6 by Coman et al. [56]. However, on the calorimetric study of Wang et al. using C-80, a cluster of relatively higher values of E_a and log A were fitted, for example, especially the respective 498.5 kJ mol^{-1} and 61.3 in the reaction of $Li_{0.5}CoO_2$ with DEC were determined [92]. A special but rare deconvolution-based peak separation has been asserted by Ping et al. [22], the complicated and overlapped thermal curve related to reaction of Li_xCoO_2 with electrolyte were deconvoluted into five single step reactions with its individual Arrhenius parameters. Individual Arrhenius parameters of Li_xCoO_2 reacted with electrolyte or organic carbonates are depicted in Table 5 [22,25,27,29,56,92]. Fig. 3 correlated the relation of E_a versus log A in reaction of Li_xCoO_2 with electrolytes.

4.4. Thermoanalytical kinetics of decomposition of electrolytes

It was believed that the decomposition of organic carbonates played the important roles in the thermal and pressure hazards of the thermal runaway of a commercial lithium-ion battery. Only several reports regarding kinetic parameters on the decomposition of electrolytes have been announced. Arrhenius parameters of E_a and log$A$ proposed by Coman and Spotnitz & Franklin are given in Table 6 [26,30,56]. An use of MRSST(Modified Reactive System Screening Tool) to verify the thermal stability and decomposition for electrolytes for lithium-ion batteries was demonstrated by Botte et al. [18]. EC and ethyl methyl carbonate (EMC) were found to decompose at the temperature of 263 and 320 °C and generated the non-condensable gases of CO_2, H_2 and O_2. In their prior study, 23 formulations of electrolytes were studied by DSC, the majority of the exothermic temperatures were higher than 205°C and the released heat were less than 300 J g^{-1} [18]. Due to the composite form and intimate contact with cathode material, oxidation or decomposition of electrolytes with Li_xCoO_2 must be recognized to be coupled together. Therefore, Arrhenius parameters on the decomposition of electrolytes are merged into the section for reaction of Li_xCO_2 with electrolyte.

4.5. Thermoanalytical kinetics on a commercial 18650 LIB containing cathode material of $LiCoO_2$

Driven by the interests in kinetics, to the world-wide extensive works on commercial 18650 batteries containing the cathode material of $LiCoO_2$ have been enthusiastically devoted. Several laboratories reported the chemical kinetics of $LiCoO_2$ battery. On the different way to the autocatalytic model emphasized by Dahn's group, only the n-th order reactions were proposed. Four brands of batteries were produced by LG, SAMSUNG, Sanyo and SONY after fully charged at 4.2 V, Jhu et al. propounded that the E_a values distributed in the range from 125.4 to 164.0 kJ mol^{-1} and log A (A in sec^{-1}) spread from 11.8 to 16.0 [16]. However, when charged to 3.7 V without indicating the SOC, the E_a values spanned in the range from 125.4 to 193.0 kJ mol^{-1} and log A (A in sec^{-1}) dispersed from 10.9 to 18.9. The bizarre and large distributions within the E_a and log A were not explained by Jhu et al. when the OCV was charged to 3.7 V [16]. In next year for the same SONY 18650 battery at full charge, a set of different Arrhenius parameters E_a and log A being 135.1 kJ mol^{-1} and 12.7 under thermal runaway were obtained [93]. In 2016 similar exploration on the common SONY 18650 battery, the kinetics of thermal runaway with the SOC of 100%, 80% and 50% were the targets of study, however, the totally different two stage mechanisms associated with E_a and log A within the thermal runaway of SONY $LiCoO_2$ batteries were claimed [17]. E_a spanned from 108.1 to 682.1 kJ mol^{-1} and log A dispersed from 3.0 to 25.8 [17]. To our knowledge, log A = 3.0 is too low to be reasonable and E_a = 682.1 kJ mol^{-1} is too high to be acceptable. These data are explicitly outside the scale of physics under the consideration either by reaction dynamics and transition state theory. Some drastically paradoxical results concerning the thermal runaway of SONY 18650 batteries were flawed. Ping et al. created a unique method for the complicated and overlapped thermal curve related to the runaway reaction of Li_xCoO_2 battery, the lumped thermal curve were deconvoluted into six single step reactions with its individual Arrhenius parameters [22]. Besides, such astonishing deviations in activation energies and frequency factors are far away from the suggested uncertainties in ASTM E2041 or ASTM E 2781 [59,70]. After the discrimination of false results of kinetic parameters by the standards of ASTM E2041 and E 2781, for the $LiCoO_2$ cathode batteries, the average activation energy is pretty certain at about 135.1 kJmol^{-1} which exhibit excellent agreement with those results quantified by MacNeil et al. [13,14]. Escobar-Hernandez has also pointed out the kinetic parameters of the SONY 18650 battery with the reaction order of 1.16, E_a of 214.6 kJ mol^{-1}, and logA of 19.0 [94]. The published activation energies and frequency factors of the Arrhenius parameters on thermal runaway of 18650 $LiCoO_2$ batteries are listed in Table 7 and shown in Fig. 4.

Table 4
Kinetic parameters on thermal decompositions of Li_xCoO_2 [20,30,91]

Cathode Material	Open Circuit Voltage (V)	Calorimeter /Spectrometer	Order (n)	E_a (kJ mol^{-1})	Log A (sec^{-1})	Reference
$Li_{0.81}CoO_2$	NA	TPD-MS	NA	130.0	NA	[20]
$Li_{0.65}CoO_2$	NA	TPD-MS	NA	97.0	NA	[20]
Li_xCoO_2	NA	TGA	NA	148.9	NA	[91]
Li_xCoO_2	NA	C-80	NA	88.9	NA	[91]
Li_xCoO_2	NA	Fitted	NA	122.2	11.8	[30]

Note: NA, Not available

Table 5
Kinetic parameters of Li_xCoO_2 with electrolytes [22,25,27,29,56,92]

Cathode Material	Electrolyte	Calorimeter/Spectrometer	Order (n)	E_a (kJ mol^{-1})	Log A (sec^{-1})	Reference
Li_xCoO_2	1.0MLiPF$_6$/EC + DEC(1:2.2)	C-80	NA	a:241.9 b:420.5 c:493.4 d:670.1 e:630.9	a:34.0 b:47.5 c:52.2 d:132.0 e:62.6	[22]
Li_xCoO_2	1.0MLiPF$_6$/EC + DEC(1:1)	C-80	NA	a:153.6 b:389.9 c:482.7 d:712.4	a:16.2 b:34.0 c:27.7 d:68.2	[22]
Li_xCoO_2	Electrolyte	NA	NA	122.5	11.8	[25]
Li_xCoO_2	Electrolyte	NA	NA	139.6	13.8	[27]
Li_xCoO_2	Electrolyte	NA	NA	139.6	13.8	[29]
Li_xCoO_2	Electrolyte	Fitted	NA	122.2	13.6	[56]
$Li_{0.5}CoO_2$	EC	C-80	NA	229.9	23.3	[92]
$Li_{0.5}CoO_2$	PC	C-80	NA	321.9	33.5	[92]
$Li_{0.5}CoO_2$	DEC	C-80	NA	498.5	61.3	[92]
$Li_{0.5}CoO_2$	DMC	C-80	NA	258.3	30.0	[92]
$Li_{0.5}CoO_2$	EMC	C-80	NA	452.2	57.4	[92]

Note: NA, Not available

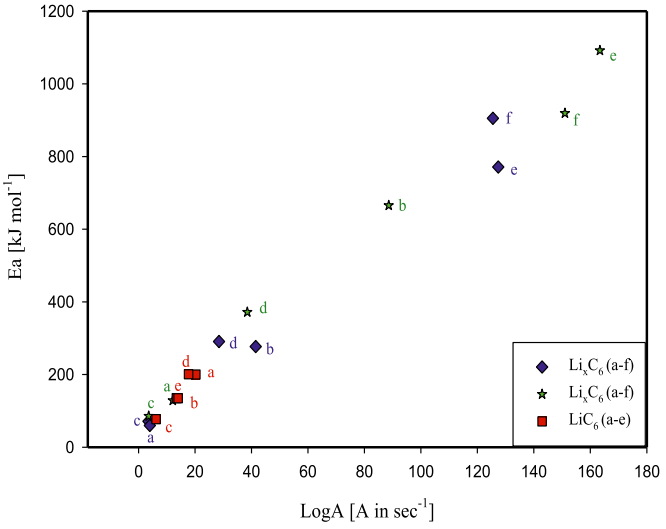

Fig. 3. Relation of activation energy versus log$A$ regarding Li_xCoO_2 reacted with electrolyte

Table 6
Kinetic parameters on decomposition of solvent in electrolyte [26,30,56]

Component in electrolyte	Calorimeter/ Method	Order (n)	E_a (kJ mol^{-1})	Log A (sec^{-1})	Reference
Solvent	ARC	NA	274.0	25.7	[26]
Solvent	Fitted	NA	105.4	10.2	[30]
Solvent	Fitted	NA	95.1	10.7	[56]

Note: NA, Not available

4.6. Window of kinetic triplets suggested by standard tests of ASTM

4.6.1. Standard deviations and kinetics window

Thermoanalytical methods of DSC, ARC, GTA and differential thermal analyzer (DTA) provide a bulk or lumped signal of all elementary reactions occurring in the thermal analysis. In DSC and ARC, the respective conversion can be presented as consumption of enthalpy change and relative to temperature rise. Similarity, for TGA, the conversion is proportional to the function of mass loss. For the same sample but analyzed by different calorimetry, the functions of conversion relative to temperature or rate are different more or less. Once the kinetic verification is started for the thermal runaway of a lithium-ion battery, modeling the rate equation and mechanism is necessary for assuring the correctness of the hypothetical model. From this viewpoint, the first step is precisely and accurately to present the kinetic parameters using thermoanalytical techniques in controlling the standard deviations of kinetic parameters inside the ranges stressed by the standards of ASTM. Furthermore, a kinetics window related to the Arrhenius parameters was particularly stressed to be followed in the ranges: order from 0-th to second order, E_a from 50 to 250 kJ mol^{-1}, and log A from 8 to 30 [59]. All the homogeneous n-th order reactions anticipating that the value of n greater than 2 or that the order not simple integer such as 2.5 or 0.7 as well as the log A not in the range from 8 to 25 must be re-checked carefully by considering the physical meaning of chemical physics or reaction dynamics [59]. Most of kinetics studies in a whole battery or its components, the reaction orders were omitted due to the complexity of solid-state reaction, which can delicately be verified by means of conventionally instrumental analysis and time-consuming chemical analysis. An E_a value of 500 kJ$mol^{-1}$is higher than the typical bond dissociation energy of C-H (412 kJ mol^{-1}) or C-C (348 kJ mol^{-1}), such a high E_a should be rechecked for its physical meaning or more practically a non-existed data or false results. A data judged to be accurate, precise and acceptable or not was based on the bias of individual parameter less than the uncertainties recommended by the ICTAC committee and standards of ASTM [59,60,70,71]. A window of rational Arrhenius parameters with good precision suggested by the standard tests of ASTM and ICTAC committee can be rearranged in Table 8 [59,60,70,71]

4.6.2. Frequency factor from simple collision and transition state theory

In simple collision theory, by the negligence of the steric factor, frequency factor can be expressed as $A = \Omega < v >_{rel}$. Ω is the reaction cross section and $< v >_{rel}$ is the relative velocity between reactants. With an assumption of Li with organic carbonate (representing the reaction of Li_xC_6 with organic carbonate in electrolyte) or reaction of oxygen with organic carbonate (representing the reaction of cathode decomposition to liberate oxygen and react with electrolyte), a cross section is taken to be 600 $Å^2$ and relative velocity to be 650 m sec^{-1} at 200 °C, thus, frequency factor A is determined to be 3.9×10^{-15} m^3 sec^{-1} or 2.3×10^{12} M^{-1} sec^{-1} which corresponds to log A = 12.4. Another foreseeable picture by transition state theory, in the systems of solution or unimolecular reaction, the frequency factor can be expressed as $A = (kTe/h)\exp(\Delta S^{0\neq}/R)$, in which k is the Boltzmann constant; T is absolute temperature; e is the exponential; h is the Planck constant; $\Delta S^{0\neq}$ is the standard entropy change of activation; R is the universal gas constant. By taking T to be 200 °C and $\Delta S^{0\neq}$ to be 20 J

Table 7
Kinetic parameters of commercial 18650 LIB [16,17,22,93,94]

LIB	OCV(V)/SOC(%)	Cathode material	Calorimeter/Spectrometer	Order (n)	E_a (kJ mol^{-1})	Log A (sec^{-1})	Reference
LG	4.2 V	$LiCoO_2$	VSP 2	NA	154.4	15.8	[16]
SAMSUNG	4.2 V	$LiCoO_2$	VSP 2	NA	125.4	11.8	[16]
Sanyo	4.2 V	$LiCoO_2$	VSP 2	NA	164.0	16.0	[16]
SONY	4.2 V	$LiCoO_2$	VSP 2	NA	125.4	11.9	[16]
LG	3.7 V	$LiCoO_2$	VSP 2	NA	193.0	18.9	[16]
SAMSUNG	3.7 V	$LiCoO_2$	VSP 2	NA	125.4	11.3	[16]
Sanyo	3.7 V	$LiCoO_2$	VSP 2	NA	164.0	14.8	[16]
SONY	3.7 V	$LiCoO_2$	VSP 2	NA	125.4	10.9	[16]
SONY	100 %	$LiCoO_2$	VSP2	NA	111.9	12.2	[17]
SONY	100 %	$LiCoO_2$	VSP2	NA	682.1	8.08	[17]
SONY	80 %	$LiCoO_2$	VSP2	NA	108.1	11.3	[17]
SONY	80 %	$LiCoO_2$	VSP2	NA	580.8	6.7	[17]
SONY	50 %	$LiCoO_2$	VSP2	NA	225.8	25.8	[17]
SONY	50 %	$LiCoO_2$	VSP2	NA	173.7	3.0	[17]
SONY	30 %	$LiCoO_2$	VSP2	NA	212.3	22.7	[17]
A	4.2 V	$LiCoO_2$	C-80	NA	a:443.3	a:76.3	[22]
					b:59.7	b:4.0	
					c:71.2	c:3.5	
					d:521.8	d:57.9	
					e:489.3	e:82.1	
					f:478.6	f:66.4	
					g:1091.9	g:146.3	
					h:829.0	h:175.8	
					i:381.0	i:140.4	
B	4.2 V	$LiCoO_2$	C-80	NA	a:130.4	a:12.4	[22]
					b:557.2	b:70.4	
					c:968.0	c:101.8	
					d:1152.1	d:87.4	
					e:549.3	e:83.8	
					f:241.0	f:18.5	
NA	4.2 V	$LiCoO_2$	VSP 2	NA	135.1	12.7	[93]
SONY	NA	$LiCoO_2$	NA	1.16	214.6	19.0	[94]

Note: NA, Not available

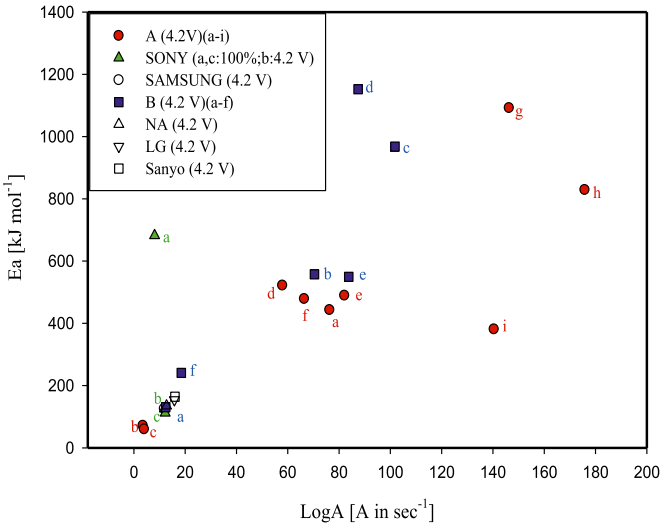

Fig. 4. Relation of activation energy versus log$A$ for 18650 $LiCoO_2$ batteries

mol^{-1} K^{-1}, A is calculated to be 8 × 10^{14} sec^{-1}, which corresponds to log A = 14.9. From simple collision theory or transition state theory the frequency should occur in the generic range of 10^8 to 10^{16} on the basis of collision rate or vibration frequency in the weakest bond of transition state. Thus, the reasonable log A will be ranged from 8 to 16, which is narrower than the range regulated by ASTM E2781.

4.6.3. Activation energy estimated from Extended Evan-Polanyi equation

In 1938 Evans and Polanyi proposed the equation suitable for a series of closely related atom-transfer reactions, nowadays, which equation has been well-known as the Evans-Polanyi (E-P) equation

Table 8
A window of Arrhenius parameters suggested by standard tests of ASTM and ICTAC [59,60,70,71]

Standard deviation/ Window	Order	E_a (kJ mol^{-1})	Log$A$ (sec^{-1})	ASTM/ ICTAC	Reference
Kinetic window	0 -2	50-250	8-30	E2781	[59]
Inter-method	< 39%	< 16%	< 25%	ICTAC	[60]
Within laboratory	< 3.0%	< 3.4%	< 6.6%	E2041	[70]
Between laboratory	< 9.8%	< 9.8%	< 22%	E2041	[70]
Within laboratory	NA	< 3.7 %	< 4.1 %	E698	[71]
Between laboratory	NA	< 6.5 %	< 8.4 %	E698	[71]

Note: NA, Not available

[95]. After their innovation, numerous attempts have been made to modify the E-P equation (named as the modified or extended E-P equation (EE-P)) [96-98] and to establish empirical and semi-empirical relationships between E_a and various ground-state properties of the reactants and products for reaction. In recent years, it has become feasible to carry out high-level ***ab initio*** molecular orbital calculations to obtain reliable geometries and energies for the structures of transition-states in the interested reactions and to compute the essential activation energies. Zeman applied the extended Evan-Polanyi equation associated with thermal analysis to evaluate the kinetic parameters of eleven inorganic azides and eighteen nitroparaffins [97,98]. Saraf et al. [99] performed the estimations on the decomposition kinetics of nineteen aromatic nitrocompounds by using bond dissociation energy approximated by the maximum enthalpy change calculated by the Chemical Thermodynamic and Energy Release Program (CHETAH) and transition-state theory (TST). Although the above EE-P equation and TST apply for reactions in the gas phase, reactions of widely different types are included and no distinction is made between gas-phase reactions and those in liquid states or solutions. In detailed discussion the

reliable kinetic data on the decomposition of solid-state calcite, Maciejewski and Reller have analyzed 168 references showing that the majority of reported values of E_a fitted into the interval from 120 to 280 kJ mol^{-1} [100]. For comparing kinetic parameters of the popular peroxy (-O-O-) bonding, the activation energies on the thermal decomposition of four dialkyl peroxides determined by various calorimetry as well as the efforts in hundred tests of experiment data were also presented in Table 9 and Fig. 5 [96-103]. As for a further moment, due to the partial double bond or mesomeric effect kept in the aromatic nitro-group, the E_a can be found to be in the range from 180 to 250 kJ mol^{-1}, these are the reasons why that the E_a larger than 250 kJ mol^{-1} and log A larger than 20 are both suggested to be reevaluated thoroughly.

4.7. Thermoanalytical kinetics

By integrating and modifying the proposed three stages, five stages or $\{T_1,T_2,T_3\}$ model of thermal runaway in commercial lithium-ion batteries from previous studies [15,25,33,40,43,104,105], according to the maximum self-heat rates exceeded 5000°Cmin^{-1} after the crucial temperature at about 200°C of commercial lithium-ion batteries under thermal runaway. An improved model of six stages including electrochemical conversion and internal short circuit induced combustion was proposed to correlate the trajectory and propagation of the exothermic reactions leading to thermal runaway in lithium-ion battery from low to high temperature as follows:

I Stage of electrochemical reaction in charge and discharge: from -60 to 60 °C
II Stage of thermal deterioration: from 60 to 85 °C
III Stage of SEI decomposition: from 85 to 120 °C
IV Stage of lithiated anode reacted with electrolyte: from 120 to 170 °C
V Stage of Li_xCO_2 reacted with electrolyte: from 170 to 200 °C
VI Stage of ingredient decomposition or collapse of a multi-layer structure induced by internal short circuit: from 200°C to maximum temperature.

In our previous works, the crucial temperature (T_{cr}) for six types of commercial 18650 lithium-ion batteries has been defined to be the temperature with a self-heat rate exceeding 100 °Cmin^{-1} [10,50,51]. Transition from crucial temperature to maximum temperature, more specifically, some delicate phenomena were suggested and posed in this work. Once going through the crucial temperature, the maximum self-heat rate in excess of 5000 °C min^{-1} in a near isothermal condition was observed. This phenomenon is verified by the experimental study of the large macro-short between Al of cathode to graphite of anode [65]. As a result of large current flow and poor heat transfer, the short circuit between Al and carbonaceous material was proposed the credible worst case of internal short inside the battery [65]. In less than ten seconds, the maximum temperature of the 18650 $LiCoO_2$ battery can reach the maximum temperature at about 700 °C. After the temperature arriving 600 °C, the residual reactants underwent a terminating reaction to the maximum temperature in conjunction with a declining temperature rate. To be brief, in this stage electrical-chemical conversion and internal short circuit induced combustion were believed and verified to occur [65]. In order to present the six stage phenomenon more lucid than the temperature versus time diagram, the profile of self-heat rate versus temperature was plotted to visualize the meticulous changes in the dynamic behavior of the battery during thermal runaway. Fig. 6 shows the temperature versus time for the thermal runaway related to the six stage model in a typical $LiCoO_2$ 18650 lithium-ion battery. Fig. 7 presents the self-heat rate versus temperature for the thermal runaway related to the six stage model in a typical $LiCoO_2$ 18650 lithium-ion battery.

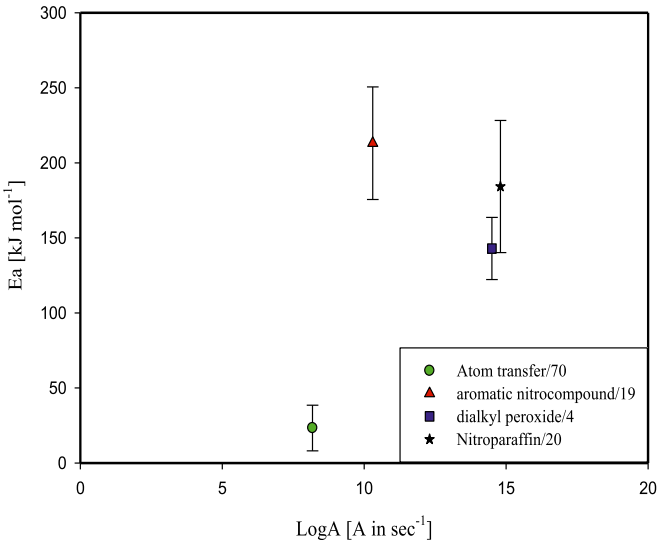

Fig. 5. Comparison of activation energy versus log$A$ among atom transfer, dialkyl peroxides and nitro-compounds

From the plot of self-heat rate versus temperature in Fig. 7, stage I to VI can be clearly visualized and distinguished from the featured self-heat rate in relation to absolute temperature. Stage I and II are non-exothermic reactions with the self-heat rate much less than 0.02 °C min^{-1}. Stage III holding the exothermic self-heat rate between 0.02 and 0.2 °C min^{-1} can be detected by ARC [11]. From stage IV to V in temperature range from 120 °C to T_{cr}, which overlapped both the reaction between electrolyte and lithiated anode as well as Li_xCO_2 associated with a self-heat rate from 0.2 to about 100 °C min^{-1} obeying the linear plot of Arrhenius equation. It is surprising that it took on a few second from T_{cr} to the point with maximum self-heat rate ($T_{max\text{-}rate}$). However, in this short time the battery passing the $T_{max\text{-}rate}$ point, which has been proclaimed to be the collapse of separator thus causing the internal Al-graphite short circuit and accelerating the violent heat-up by Joule effect [35,56,65]. Nevertheless, in stage VI from the temperature with maximum rate to about 600 °C, self-heat rate sustained in the vicinity of a maximum-rate, keeping a pseudo-static behavior in 10

Table 9
Typical activation energies determined or calculated by Evans-Polanyi Equation [96-103]

System/Entry	Evans-Polanyi (EP) or Extended Evans-Polanyi equation (EEP)	E_a(kJ mol^{-1})	Log A (A in sec^{-1})	Experimental or Theoretical	Reference
Atom transfer/70	EP	8.1-38.5	8.18	Theoretical	[96]
Decomposition of inorganic azide/11	EEP	75.3-179.9	NA	Experimental	[97]
Nitroparaffin/20	EEP	140.2-228.2	11.8-17.7	Theoretical	[98]
Decomposition of aromatic nitrocompound/19	EEP	194.3-231.8	10.3	Theoretical	[99]
Decomposition of calcite	NA	120-280	NA	Data from 168 references	[100]
Decomposition of dialkyl peroxide/4	NA	122.2-163.6	11.4-17.6	Experimental	[101,102,103]

Note: NA, Not available

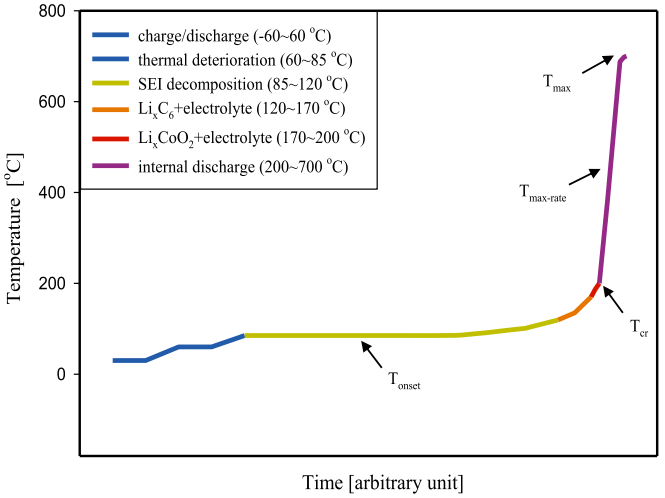

Fig. 6. Temperature runaway curve for a typical 18650 $LiCoO_2$ battery

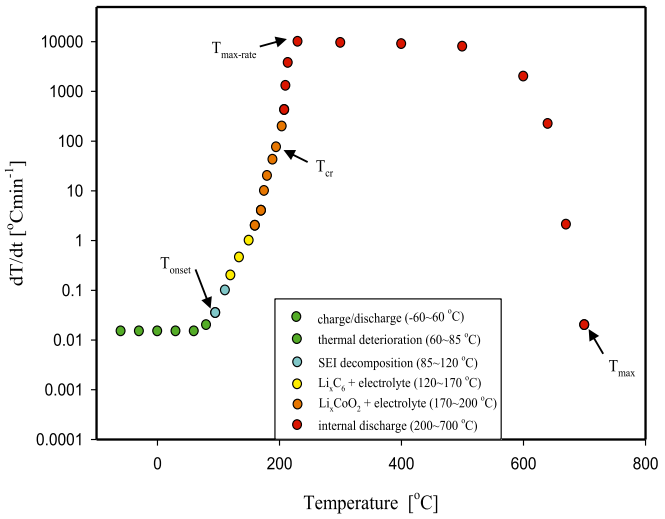

Fig. 7. The self-heat rate versus temperature for a typical 18650 $LiCoO_2$ battery under thermal runaway

second, then falling down to the completion of reaction at maximum temperature with the value of (dT/dt) approaching zero. This unique feature is deemed to be the behavior of the thermal propagation of flame after the rupture of lithium-ion battery accompanying the release of flammable mixture of electrolyte being auto-ignited. A thermal propagation of flame can be characterized by a smooth in the rate of exothermic reaction conjugated with the considerable increase of temperature [106], which is in excellent agreement with the relation of self-heat rate versus temperature from $T_{max\text{-}rate}$ passing the turnaround point to the T_{max} with flammable reactant exhausted.

4.7.1. Decomposition of SEI

Previous work with the ARC data on a MCMB material, Richard and Dahn have identified an exothermic peak due to the decomposition of SEI in ARC studies of carbon anodes in the electrolyte at about 100 °C to be independent of lithium content. The SEI layer is believed to consist of stable (Li_2CO_3 and LiF) and metastable components $(CH_2O\text{-}CO_2Li)_2$ [11,107,108]. The metastable SEI decomposes to stable species with small amount heat as follows:

$$(CH_2O\text{-}CO_2Li)_2 \rightarrow Li_2CO_3 + C_2H_4 + CO_2 + 1/2\ O_2 \quad (9)$$

or

$$2Li + (CH_2O\text{-}CO_2Li)_2 \rightarrow 2Li_2CO_3 + C_2H_4 \quad (10)$$

The depletion of SEI component gives rise to the knee-like peak with a tiny self-heat rate as high as 0.2 °C min^{-1}. The rate law can be assumed to be $R = -d[SEI]/dt = k\,[SEI]$, MacNeil et al. expressed the self-heat rate equation to be dependent on the concentration of SEI as x [11]:

$$\frac{dT}{dt} = \left(\frac{\Delta H}{C_p}\right)\left(\frac{dx}{dt}\right) \quad (11)$$

By obeying the n-th order reaction and Arrhenius equation, the self-heat rate equation can be written as:

$$\frac{dT}{dt} = \left(\frac{\Delta H}{C_p}\right)x^n A e^{-(E_a/RT)} \quad (12)$$

For simply equating the self-heat, setting the initial concentration x of SEI to be 1, then the logarithm of the self-heat rate can be further deduced as:

$$\ln\left(\frac{dT}{dt}\right) = \ln(A\Delta T) - \left(\frac{E_a}{RT}\right) \quad (13)$$

where ΔT is the adiabatic temperature rise can be given by $\Delta H/C_p$. By plotting the natural logarithm of the self-heat rate ln (dT/dt) versus the reciprocal of temperature $1/T$, E_a and A can be obtained from the slope and intercept, respectively. By setting ΔT = 15 °C and from the plot of ln(dT/dt) against $1/T$, an E_a of 135.1 kJ mol^{-1} and log A of 15.2 (A in sec^{-1}) were determined [11]. Chen et al. put forward that the E_a of the MCMB-1028, SMG-N-7b, SMG-N-20 and SMG-Ns-15f on the decomposition of SEI were measured respectively to be 53, 88, 92 and 78 $kJmol^{-1}$ by DSC [85].

4.7.2. Reaction of Li_xC_6 with electrolyte

By comparing the change in the profiles cause by heating to 220 °C in the ARC, Richard and Dahn found that the consumption of Li about Δx = 0.3 in Li_xC_6 [11]. The exothermic reaction continued after the tail of SEI decomposition peak, it was considered to be the reaction of Li_xC_6 with electrolyte controlled by the transport of Li through the rebuilt SEI film. They assumed that the new SEI after the charge and discharge by incoming lithium-ion and EC will reach the same thickness under steady state situation. However, after the SEI peak at about 105 °C, the quantity of lithium passed through this new SEI layer per unit time to react with electrolyte was proportional to the area of new SEI film and affected by the amount of intercalated lithium in Li_xC_6. Therefore, the self-heat rate representing the reaction rate was shown to be proportional to the surface area of new SEI on anode. This phenomenon showed that the diffusion rate of Li from Li_xC_6 to liquid state and reacted with electrolyte to decide the rate of exothermic reaction. It was very pellucid to be observed in the self-heat rate with a steady rate of 0.1 to 1.0 °C min^{-1} and steady exothermic curve detected by DSC from 110 to 220 °C [11,109]. Mukai et al. rationalized that from the DSC thermal curves the Li_xC_6 reaction with electrolyte were found to be divided into four temperature regions regardless of lithium content: region (1) below 150 °C; region (2) from 150 to 240 °C; region (3) from 240 to 270 °C; region (4) above 270°C. They claimed from DSC and X-ray data that the exothermic reaction in the region (1) and region (2) were attributed to the decomposition of SEI and formation of LiF by the reaction of electrolyte with Li diffused from Li_xC_6, respectively [11,109]. Two peaks were distinguished, the first could be attributed to the transformation of the passivated SEI film and the second peak was due to the diffusion of lithium and the subsequent reaction with electrolyte [107]. The combination of heat produced by these two reactions caused the sample temperature to increase. By this model, self-heat rate can be expressed as a combined function of (1) the amount of lithium present in the original metastable SEI (x_{f0}) which converts to stable SEI (2) the amount of intercalated lithium (x_{i0}) which is available to form

new SEI. In short, heat is produced as metastable SEI converts to stable SEI (dx_f/dt) and when lithium reacts with the EC to form new SEI (dx_i/dt). Richard and Dahn rearranged the self-heat rate equation as [11]:

$$\left(\frac{dT}{dt}\right) = \left(\frac{\Delta H_1}{C_p}\right)\left(\frac{dx_f}{dt}\right) + \left(\frac{\Delta H_2}{C_p}\right)\left(\frac{dx_i}{dt}\right) \tag{14}$$

The change in the amounts of reactants and products, x_f (thickness of SEI film), x_i (Li content in Li_xC_6), a (specific surface area) and z_i (SEI thickness) can be formulated according to Arrhenius equation:

$$\left(\frac{dT}{dt}\right) = \left(\frac{\Delta H_1}{C_p}\right)x_f^n A_1 e^{-Ea_1/RT} + \left(\frac{\Delta H_2}{C_p}\right)x_i\left(\frac{a}{a_0}\right)e^{-z/z_0}A_2 e^{-Ea_2/RT} \tag{15}$$

where ΔH_1 is the heat of reaction for the formation of stable SEI from metastable SEI, ΔH_2 is the heat of intercalated lithium diffused from Li_xC_6 through SEI to react with EC, C_p is the heat capacity of the sample containing test tube, the expression of $(\Delta H_1 x_{f0}/C_p)$ and $(\Delta H_2 x_{i0}/C_p)$ are the adiabatic temperature rises for the sample if all the x_{i0} and x_{f0} are consumed. Based on the experimental results presented in Richard and Dahn [11], $A_1 = 1.25 \times 10^{17}$ min^{-1}, $E_{a1} = 1.4$ eV, $x_{f0} = 0.1$, $x_{f0} = 0.16$, $\Delta H_1/C_p = 150$°C and $\Delta H_2/C_p = 325$°C. In the above equation, the exact values for E_{a2} and A_2 are unknown quantities, by using a series of trial calculations showed that a range of values for E_2 and A_2 would produce an acceptable fit to the measured ARC results. For the tunneling of lithium penetrating through the new SEI film E_2 was chosen as 0.37 eV and A_2 was 70 min^{-1}, and for the transport behavior of lithium E_{a2} was chosen as 0.8 eV and A_2 as 10^8 min^{-1} [12]. A group of similar results was provided by Yang et al. [86], they used DSC and the Kissinger method to verify the kinetic parameters of the reaction between $Li_{0.91}C_6$ (GDR),$Li_{0.71}C_6$ (Mag-10), $Li_{0.91}C_6$ (Mag-10) and electrolytes.

4.7.3. Reaction of Li_xCoO_2 with electrolyte

As described above, it is known that the reaction for cathode material decomposition is coupled or overlapped with that of solvent oxidation. Delithiated lithium cobalt oxide could (1) directly react with solvent, however, this mechanism of oxidation reaction is still not clear; or (2) disproportionate to give off oxygen that reacts with solvent. Even the famous equation for the thermal decomposition of Li_xCO_2 to liberate oxygen at temperatures higher than 250°C to react with electrolyte, several researchers have reported that the exothermic onset temperature of Li_xCO_2 with electrolyte can be as low as 150 °C [19,92,110]. This process has been characterized already, the reaction of electrolyte with Li_xCO_2 may be caused by the oxidation of solvent below 170 °C owing to the CoO structure in Li_xCO_2 detected by X-ray diffraction (XRD) [89]. When the temperature exceeding 250 °C, Li_xCO_2 decomposed and released oxygen to react with organic carbonates accompany the release of CO_2 and H_2O. MacNeil and Dahn studied the reaction kinetics for Li_xCO_2 in non-aqueous electrolyte, an E_a of 123.5 kJ mol^{-1} and a log A (A in sec^{-1}) of 11.8 were reported [13,14]. Wang et al. have applied the thermoanalytical technique associated with the thermal curves obtained from C-80 calorimeter as well as the method of Borchardt & Daniels to determine the E_a and A in the reaction system of delithiated cathode materials and electrolytes [21,22]. By assuming the first order reaction and due to the complex thermal curve of the reaction in Li_xCoO_2 and electrolytes, it is explicit that the E_a and log$A$ determined by Wang et al. have the larger deviations and less precision in comparison to Arrhenius parameters reported by other researchers.

4.7.4. Electrical-chemical conversion by internal short circuit

Both the exothermic reactions of the electrolytes reacted with anode and cathode materials have been suspected to be the sources which give birth to the runaway reaction under abusive conditions. Nowadays, the published results with striking disputes among the reported phenomena in relation to the severe thermal runaway [5,15,16,29,49,58]. Jhu et al. exaggerated that the thermal runaway occurred in 18650 $LiCoO_2$ batteries being a thermal explosion without the requisite evidences to prove the model to be correct [16]. Conventionally, the violent thermal runaway was deduced to be the reaction of electrolytes with O_2 released from the destruction of Li_xCoO_2 above 250 °C [89-91]. For the past few years, the initiation and propagation of thermal runaway have been proved by high-speed tomography and by internal discharge using direct short between Al of cathode and graphite of anode [10,35,56,65]. Disastrously, it is certainly lacked of both qualitative and quantitative studies that have ever been performed experimentally to identify the tremendous self-heat rate originated from. Internal short induced thermal response is a problem of three dimensional multi-physics which depend on nature of short, cell capacity, open circuit voltage, electrical design, internal structure, reaction kinetics and electrochemical property. The overall heat from short circuit is composed of the global heat from discharge in whole circuit and local heat at the internal short point. Kim et al. created the multi-physics models of internal short-circuit and microscopic mechanisms to explain the thermal response of lithium-ion battery [111]. A medium resistance short between Al and LiC_6 (graphite) with resistance at approximately 0.01 ohm by passing the cathode can generate the short current as high as 300A which can easily result in the fire and explosion of lithium-ion battery. The temperature at 10 sec after the internal Al-LiC_6 short can even as high as 600 °C on Al tab [111]. However, it is a regret that in this region, there is no proposed kinetics for fitting together with the sudden temperature rise and tremendous self-heat rate exceeding 5000 °C min^{-1} inside the diverse lithium-ion batteries.

4.7.5. Autocatalytic reaction between Li_xCoO_2 and electrolytes

For solid-state reactions, the basics and models have been reviewed by Khawam and Flanagan [48]. Model deviation is based on several proposed reaction mechanisms which include n-th order reaction, nucleation, geometric shape and diffusion. Šesták and Berggren have derived a mathematical form that represents all mechanism in a single expression [112]:

$$f(\alpha) = \alpha^m(1-\alpha)^n[-\ln(1-\alpha)]^p \tag{16}$$

MacNeil et al. facilitated the technique of ARC to study the exothermic reaction between Li_xCoO_2 and electrolyte [13]. A novel observation of the exothermic phenomenon with an autocatalytic feature has been verified, even until now, this is the first autocatalytic model proposed to explain both the ARC and DSC results [13]. They observed that the self-heat rate did not obey the Arrhenius-like line in the plot of $\ln(dT/dt)$ versus $1/T$, the behaviors of dT/dt were discovered to be accelerated by the presence of products. A comprehensive autocatalytic reaction used to develop chemical kinetics linking with a corresponding rate equation can thus be represented as

$$\left(\frac{d\alpha}{dt}\right) = k(1-\alpha)(\beta + \alpha^{0.5}) \tag{17}$$

where α is the degree of conversion, and β is the autocatalytic parameter determined by simulation. The self-heat rate regarding the overall autocatalytic reaction between Li_xCoO_2 and electrolyte can be described by:

$$\left(\frac{dT}{dt}\right) = \left(\frac{\Delta H}{C_p}\right)\left(\frac{d\alpha}{dt}\right) \tag{18}$$

Soon after the announcement of autocatalytic model, another similar model was also cited by MacNeil and Dahn, a method has been developed to discriminate the reasonable conversion function $f(\alpha)$ from the sixteen default models [14]. An “universal” equation was expressed to describe their observation on thermal runaway of a $LiCoO_2$ battery:

$$\left(\frac{d\alpha}{dt}\right) = k\alpha^m(1-\alpha)^n[-\ln(1-\alpha)]^p \tag{19}$$

where the m, n, and p are partial reaction order for the autocatalytic

decomposition, and α_0 is the initial conversion. The variables in the above equation can be selected for most solid-state decomposition with the mechanisms applicable for any one of the diffusion, *n*-th order, or autocatalytic reactions and their combinations. They had demonstrated that the all-fit, Grewer 13 and model 12 could precisely describe the initial reaction of Li_xCoO_2 and electrolyte using both ARC and DSC profiles. A higher degree of confidence was reserved for these three conversion functions which modeled the self-heat rate in ARC and thermal curve in DSC very well with the kinetic parameters featured in Table 10. However, the minor defect was that the both simulated data of DSC profile and of the ARC self-heat rate were limited in the temperature range from 150 to 225 °C, which covered merely the stage IV and V as what mentioned above [10,13,14,25].

Hatchard et al. followed the calorimetric data for Li_xCoO_2 reaction with electrolyte, a hypothetical reaction kinetics for autocatalytic model was presented in thermal abuse model [25]. Tables 10a, 10b and 10c depict that ten studies have established the similar models for the purposes of designing better and safer lithium-ion batteries [14,25,27-30,33,36,57,113].

4.8. Thermal kinetics of electrode materials and whole commercial 18650 lithium-ion batteries

A precise reaction kinetics for a particular reaction can be well-defined if the kinetic triplets ($f(\alpha)$, E_a and A) being extracted accurately from various experimental techniques. Even with a good discussion of accountability of the kinetic triplets and the best-fitted f(**α**) does not guarantee the catch of reaction mechanism or parameters of activation in transition state theory. In general, the reaction order was neglected for a solid-state reaction studied by DSC and ARC, thermoanalytical kinetics usually provided E_a and log *A*. The most informative part among order, E_a and log *A* is believed to be the experimental value of E_a, which can interpret the characteristics in a peculiar reaction between Li_xCoO_2 and the electrolyte. Fig. 8 depicts all the E_a and log A in regards to 18650 $LiCoO_2$ battery and its components. E_a distributes from 50 to 1150 kJ mol^{-1}. Log *A* (*A* in sec^{-1}) has the data spread from 1 to 170. It is astonishing that both the E_a and log *A* have such tremendous data range or inconsistency. It is worthy to have a transparent understanding on the accuracy and precision of these kinetic parameters relative to the battery and its components.

Table 10b
Kinetic parameters of the reaction of Li_xCoO_2 and electrolyte of autocatalytic model I [13]

Sample	Charged voltage (V)	E_a (kJ mol^{-1})	Log*A* (sec^{-1})	β	Reference
1	4.1	154.4	14.5	0.15	[13]
1	4.2	154.4	14.5	0.2	[13]
1	4.3	154.4	14.7	0.25	[13]
2	4.1	144.7	13.6	0.15	[13]

Note: In Table 10 (b) the average activation energy and frequency factor in log*A* are 152.0 ± 4.2 kJ$mol^{-1}$and 14.3 ± 0.4, respectively.

Table 10c
Kinetic parameters of the reaction of Li_xCoO_2 and electrolyte of autocatalytic model II [14,27]

Model	E_a (kJ mol^{-1})	Log*A* (sec^{-1})	*m*	*n*	*p*	α_0	Reference
All-fit	123.9	11.4	0.26	1.6	0.49	0.04	[14]
Model 12	119.8	10.8	0.0	1.0	2/3	0.03	[14]
Grewer 13	124.6	11.2	0.5	1.0	0.0	0.04	[14]
Kim et al.	139.6	13.8	1.0	1.0	0	none	[27]

Note: In Table 10 (c) the average activation energy and frequency factor in log*A* are 127.0 ± 7.5 kJ $mol^{-1}$and 11.8 ± 1.2, respectively.

In transition state theory, the activation energy depending on the enthalpy of activation ($\Delta H^{0\neq}$) has no relation to the dynamics-related frequency factor. The cause of isokinetic effect can be attributable to chemical or physical factors or can arise from the computational artifact. Because fitting experimental data to a rate equation is usually accomplished by simultaneously adjusting the values of *A* and E_a, the values should be correlated in a compensating manner so that their simultaneous changes do not change the rate. In early studies, a so-called isokinetic effect (or compensation effect) has been observed and widely adopted [114-116]. Generally, this effect can be expressed by a linear relation as $\log A = aE_a + b$, where a and b are constants. Fig. 8 depicts the experimental values of E_a and log*A* for the thermal runaway of $LiCoO_2$ battery system, the data trend shows a very strong correlation of compensation effect between E_a and log*A*. It makes sense from Fig. 8 that the experimental value of E_a is by far more narrow than the value of log*A*. By simple figuring, a tolerable bias in E_a by 20% from 125 to

Table 10a
Auto-catalytic models of delithiated cathode materials reacted with electrolyte [14,25,27-30,33,36,57,113]

Authors	Auto-catalytic Model	Referred sources of kinetic model and parameters
Hatchard et al.[a] (2001) [25]	$\frac{d\alpha}{dt} = A_c\alpha^m(1-\alpha)^n[-\ln(1-\alpha)]^p \exp(-\frac{E_{a,c}}{RT})$, $m = n = 1$, $p = 0$	Richard & Dahn [14]
Kim et al. [b] (2007) [27]	$\frac{d\alpha}{dt} = A_c\alpha(1-\alpha)\exp(-\frac{E_{a,c}}{RT})$	Richard & Dahn [14]
Lopez et al.[c] (2015) [28]	$\frac{d\alpha}{dt} = A_c\alpha(1-\alpha)\exp(-\frac{E_{a,c}}{RT})$	Hatchard et al. [25]
Lee et al. (2015) [36]	$\frac{d\alpha}{dt} = A_c(1-\alpha)(\alpha+\beta)\exp(-\frac{E_{a,c}}{RT})$	Fitted with ARC data
Coman et al. (2016) [30]	$\frac{d\alpha}{dt} = A_c\alpha(1-\alpha)\exp(-\frac{E_{a,c}}{RT})$	Hatchard et al. [25]
Yayathi et al. (2016) [113]	$\frac{d\alpha}{dt} = A_c\alpha(1-\alpha)\exp(-\frac{E_{a,c}}{RT})$	Hatchard et al. [25]
Peng et al. (2016) [29]	$\frac{d\alpha}{dt} = A_c\alpha(1-\alpha)\exp(-\frac{E_{a,c}}{RT})$	Hatchard et al. [25]
Parhizi et al. (2016) [57]	$\frac{d\alpha}{dt} = A_c\alpha(1-\alpha)\exp(-\frac{E_{a,c}}{RT})$	Hatchard et al. [25]
Ping et al. (2018) [33]	$\frac{d\alpha}{dt} = A_c\alpha^m(1-\alpha)^n[-\ln(1-\alpha)]^p \exp(-\frac{E_{a,c}}{RT})$	Hatchard et al. [25]

Note:
[a] $Q_{thermal\ abuse} = Q_{sei} + Q_{ne} + Q_{pe}$
; $E_{a,\ sei} = E_{a,ne}$
; only the lowest part below 200°C of three separate exotherms in the ARC and DSC data for $LiCoO_2$ has been modeled and included in the simulations.
[b] $Q_{thermal\ abuse} = Q_{sei} + Q_{ne} + Q_{pe} + Q_{ele} + Q_{nb}$
; Q_{ele} was proposed by Kim et al., $E_{a,\ ele}$ and $A_{\ ele}$ are cited from the work of Spotnitz and Franklin [26].
[c] $Q_{thermal\ abuse} = Q_{sei} + Q_{ne} + Q_{pe} + Q_{ele}$
; Lopez et al. suggested that an electrolyte combustion reaction must be included in the energy model [28].

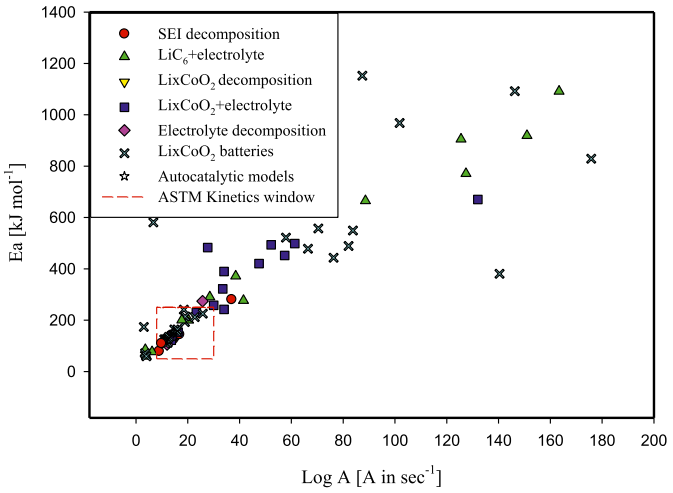

Fig. 8. Comparison of activation energy versus log*A* for 18650 $LiCoO_2$ battery and its components

150 kJ mol^{-1} can lead to the huge change in *A* at least 4 orders of magnitude from 10^{12} to 6.6 × 10^{15} sec^{-1}. This is the very reason, E_a makes itself more informative than *A*, then spending extensive efforts on E_a and treating log *A* as a subordinate parameter. The most informative part of the kinetic parameters turns out to be the activation energy. The validity of the isokinetic effect (compensation effect) in the field of kinetics analysis has been debated enthusiastically. Besides, the compensation trends have also been reported by the ICTAC kinetics project [117]. In this study, Figs. 1, 2, 3, 4, and 8 display explicitly the isokinetic effect kept within these five figures.

For the above mentioned sections, Table 11 integrates and averages the E_a and log *A* of electrode materials and whole commercial 18650 $LiCoO_2$ lithium-ion batteries. (Table 11a) lists the kinetic parameters of the electrode materials and commercial 18650 $LiCoO_2$ lithium-ion batteries obeying the bias of ASTM E2781. (Table 11b) lists the kinetic parameters of the electrode materials and commercial 18650 $LiCoO_2$ lithium-ion batteries obeying the bias suggested by ICTAC. By obeying the regulated bias and standard deviations, Fig. 9 shows the averaged E_a versus log *A* diagram which reveals that the kinetic parameters of the whole 18650 lithium-ion battery resembles the kinetic parameters of delithiated cathode reacted with electrolyte much more than those of the anode systems. Having adopted the regulations of standard deviation suggested by ICTAC, Fig. 10 gets the similar results as in Fig. 9, the averaged E_a versus log *A* diagram which reveals that the kinetic parameters of the whole 18650 lithium-ion battery resembles the kinetic parameters of delithiated cathode reacted with electrolyte much more than those of the anode systems. The authors achieve a concise viewpoint, the chemical kinetics for the thermal runaway of a 18650 $LiCoO_2$ battery under thermal abuses is close to that of Li_xCoO_2 reacted with electrolyte.

4.9. Future works on the chemical kinetics of $LiCoO_2$ battery

On the whole, the paradox and discrepancy observed on the chemical kinetics can be summed up as follows:

(a) The accuracy and precision of chemical kinetics from calorimetric studies need to be improved.
(b) Arrhenius equation suits for homogeneous reaction but is not fitted in chemical kinetics of lithium-ion battery containing solid-stated anode and cathode.
(c) From 1999 to nowadays, MacNeil and Dahn proposed two autocatalytic models for the reaction of Li_xCoO_2 with electrolyte, more extensive explorations on the solid-state reactions (for example Eq. (15)) are eagerly anticipated.
(d) Hundreds of researchers devoted themselves to study the chemical kinetics of exothermic reactions using adiabatic calorimetry, the thermal inertia has been well-known in warping the kinetics calculations and needed to be corrected to unity. Thermal inertia is suggested to be well-controlled as low as 1.05 - 1.2. Most of the kinetic studies on lithium-ion batteries ignored the correction of thermal inertia in experiment and calculation. Only some of the thermal inertia of 18650 or commercial batteries were reported.
(e) The interference of an internal short circuit from the breakdown of separator under thermal abuse and the electrical field of OCV should be avoided.
(f) Following the Townsend's theory in acquiring the kinetic parameters from data of adiabatic calorimeter, a linear fitted line can thus be obtained by selecting a correct n in advance, thereon E_a (kJ mol^{-1}) and *A* (sec^{-1} M^{1-n}) will be correctly discriminated from a straight line of ln (d*T*/d*t*) vs. 1/T without the distorted effects owing to thermal inertia larger than 1.2.
(g) Due to the difficulty in taking apart of the battery's components in glove box, the mass of the battery's material was approximetely 100 - 200 mg used in adiabatic calorimeter, which led to the thermal inertia much greater than unity thus probably distorted the acquired kinetic parameters.
(h) Three ASTM standards regulate the thermal curve have to be a simple curve for evaluating chemical kinetics. Therefore, using either the Flynn/Wall/Ozawa, Borchardt & Daniels, Kissinger methodology should confirm the appropriateness of these approaches for studying chemical kinetics involving solid-state species.
(i) More intensive studies are needed to examine the T_{cr} with a gigantic self-heat rate jump and the puzzling $(dT/dt)_{max}$ as high as 10000 °C min^{-1} which are arisen from physical or chemical phenomena.

5. Conclusions

A review focused on the thermal kinetics of the thermal runaway for an 18650 $LiCoO_2$ battery and the exothermic reactions in its components has been summarized and discussed. Most of these kinetic parameters derived from adiabatic and heat-flow calorimeters, a very few of them fitted from electrochemical-thermal model associated with ARC data. However, due to the complexity of solid-state reaction involving both anode and cathode as well as the difficulty to determine the order of reaction by chemical analysis on the surface of solid electrode, most of the interpretations of calorimetric data in order was absent or set the order to be unity for simplicity. As a whole all the kinetic parameters are depicted in Fig. 8, E_a distribute from 53 to 1152 kJ mol^{-1} and log *A*

Table 11a
Kinetic parameters of the electrode materials and commercial 18650 $LiCoO_2$ lithium-ion batteries obeying the kinetics window of ASTM E 2781.

System	Model	E_a (kJ mol^{-1})	Log*A* (A in sec^{-1})	Data source
SEI decomposition	n-th order	126.0 ± 50.6	14.4 ± 2.6	Table 2
Li_xC_6 + electrolyte	n-th order	134.4 ± 43.9	16.4 ± 2.8	Table 3
Li_xCoO_2 + electrolyte	n-th order	150.8 ± 40.3	15.3 ± 4.1	Table 5
Li_xCoO_2 + electrolyte	Autocatalytic model I	152.0 ± 4.2	14.3 ± 0.4	Table 10
Li_xCoO_2 + electrolyte	Autocatalytic model II	127.0 ± 7.5	11.8 ± 1.2	Table 10
18650 battery	n-th order	157.2 ± 38.0	14.9 ± 4.7	Table 7

Table 11b
Kinetic parameters of the electrode materials and commercial 18650 $LiCoO_2$ lithium-ion batteries obeying the suggestion of ICTAC

System	Model	*Ea* (kJ mol^{-1})	Log*A* (A in sec^{-1})	Data source
SEI decomposition	n-th order	127.2 ± 20.2	14.4 ± 2.6	Table 2
Li_xC_6 + electrolyte	n-th order	128.7 ± 12.0	16.4 ± 2.8	Table 3
Li_xCoO_2 + electrolyte	n-th order	130.9 ± 8.6	13.3 ± 0.8	Table 5
Li_xCoO_2 + electrolyte	Autocatalytic model I	152.0 ± 4.2	14.3 ± 0.4	Table 10
Li_xCoO_2 + electrolyte	Autocatalytic model II	127.0 ± 7.5	11.8 ± 1.2	Table 10
18650 battery	n-th order	136.8 ± 18.0	13.6 ± 1.7	Table 7

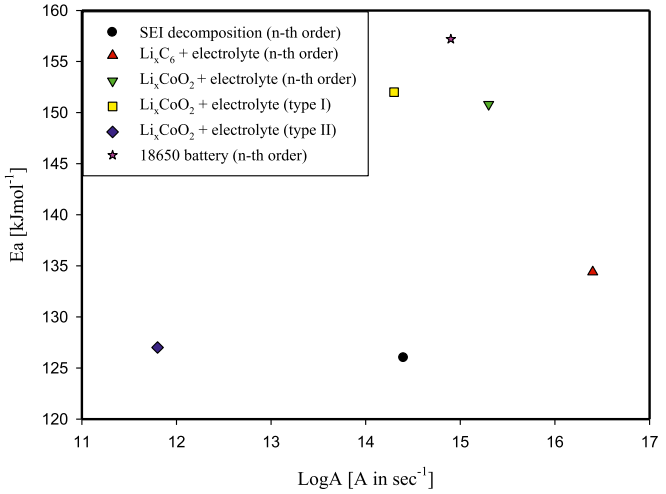

Fig. 9. The averaged E_a and Log*A* of a typical 18650 $LiCoO_2$ battery and its components obeying the kinetic window of ASTM E2781

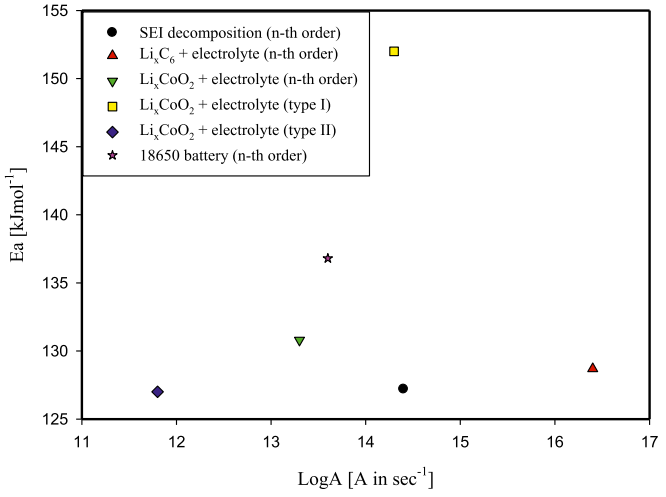

Fig. 10. The averaged E_a and Log*A* of a typical 18650 $LiCoO_2$ battery and its components following the suggestion of ICTAC

(*A* in sec^{-1}) spread from 3.0 to 175.8. A compensation effect is visualized in the E_a versus log *A* diagram with the representation of more unstable log *A*. It is of great importance to apply the accurate and precise chemical kinetics for the safety-related improvements and new designs in commercial lithium-ion batteries. All the noisy fluctuations in the battery and its components have been discriminated by both the regulation of ASTM E2781 and the suggestion of ICTAC to enhance the accuracy and precision of the kinetic parameters. Taking into account the averaged kinetic parameters from the decomposition of SEI, reaction of Li_xC_6 with electrolyte, reaction of Li_xCoO_2 with the electrolyte and the whole battery, it demonstrates that the chemical kinetics of the $LiCoO_2$ battery pretty close that of Li_xCoO_2 with electrolyte in n-th order reactions. Nevertheless, to one's surprise is that the autocatalytic model II is the popularly world-renowned in the above-mentioned thermal models does not resemble the whole battery. The paradoxical model between the n-th order and autocatalytic type regarding the reaction of Li_xCoO_2 with electrolyte is existed and has not been exactly solved. What's more, some studies in the thermal kinetics of a $LiCoO_2$ 18650 battery, the unimaginable discrepancy in the E_a ranged from 59.7 to 682.1 kJ mol^{-1} and log*A* (sec^{-1}) varied from 3.5 to 25.8, which reveals that more the extensive studies to resolve the existent atypism are urgent needs. Up to now, the trustworthy chemical kinetics of $LiCoO_2$ battery and its components is still an issue debated enthusiastically. A prospective joint effort of exceedingly better technology combining reaction dynamics, calorimetry, thermal analysis, thermodynamics and solid-state reaction for acquiring the accurate chemical kinetics of a $LiCoO_2$ battery or its ingredients will be achieved in the next few years.

CRediT authorship contribution statement

Yih-Shing Duh: Conceptualization, Data curation, Validation, Writing - original draft, Writing - review & editing. **Xinzhong Liu:** Formal analysis, Investigation. **Xuepeng Jiang:** Resources, Software. **Chen-Shan Kao:** Data curation, Software. **Lingzhu Gong:** Resources, Validation. **Ronghui Shi:** Investigation, Validation.

Declaration of Competing Interest

The manuscript has no conflict of interest.

Supplementary materials

Supplementary material associated with this article can be found, in the online version, at doi:10.1016/j.est.2020.101422.

References

[1] A. Yoshino, The birth of lithium-ion battery, Angew. Chem. Int. Ed. 51 (2012) 2–5.
[2] Y. Miao, P. Hynan, A. von Jouanne, A. Yokochi, Current Li-ion battery technologies in electric vehicles and opportunities for advancements, Energies 12 (2019) 1074–1093.
[3] P.G. Balakrishnan, R. Ramesh, T. Prem Kumar, Safety mechanisms in lithium-ion batteries, J. Power Sources 155 (2006) 401–414.
[4] C.C. Lin, H.C. Wu, J.P. Pan, C.Y. Su, T.H. Wang, H.S. Sheu, N.L. Wu, Investigation on suppressed thermal runaway of Li-ion battery by hyper-branched polymer coated on cathode, Electrochim. Acta 101 (2013) 11–17.
[5] H.M. Liu, D. Saikia, H.C. Wu, C.Y. Su, T.H. Wang, Y.H. Li, J.P. Pan, H.M. Kao, Towards an understanding of the role of hyper-branched oligomers coated on cathodes, in the safety mechanism of lithium-ion batteries, RSC Adv. 4 (2014) 56147–56155.
[6] D. Lisbona, T. Snee, A review of hazards associated with primary lithium and lithium-ion batteries, Process Saf. Environ. Prot. 89 (2011) 434–442.
[7] Exponent, SAMSUNG Recall Support Note7 Investigation Root Cause Analysis, 23 January 2017.
[8] TÜV Rheinland, Investigating Battery safety: Logistics and Assembly, 23 January 2017.
[9] UL, Failure Analysis of SAMSUNG Note 7, 23 January 2017.
[10] Y.S. Duh, K.H. Lin, C.S. Kao, Experimental investigation and visualization on thermal runaway of hard prismatic lithium-ion batteries used in smart phones, J. Them. Anal. Calorim. 132 (3) (2018) 1677–1692.
[11] M.N. Richard, J.R. Dahn, Accelerating rate calorimetry study on the thermal study of lithium intercalated graphite in electrolyte, I. Experimental, J. Electrochem.

Soc. 146 (6) (1999) 2068–2077.
[12] M.N. Richard, J.R. Dahn, Accelerating rate calorimetry study on the thermal stability of lithium intercalated graphite in electrolyte, II. modeling the results and predicting differential scanning calorimeter curves, J. Electrochem. Soc. 146 (6) (1999) 2078–2084.
[13] D.D. MacNeil, J.R. Dahn, An autocatalytic mechanism for the reaction of Li_xCoO_2 in electrolyte at elevated temperature, J. Electrochem. Soc. 147 (3) (2000) 970–979.
[14] D.D. MacNeil, J.R. Dahn, Test of reaction kinetics using both differential scanning and accelerating rate calorimeters as applied to the reaction of Li_xCoO_2 in non-aqueous electrolytes, J. Phys. Chem. 105 (2001) 4430–4439.
[15] T. Waldmann, M. Wohlfahrt-Meherens, Effects of rest time after Li plating on safety behavior-ARC tests with commercial high-energy 18650 Li-ion cells, Electrochim. Acta 1230 (2017) 454–460.
[16] C.Y. Jhu, Y.W. Wang, C.M. Shu, J.C. Chang, H.C. Wu, Thermal explosion hazards on 18650 lithium ion batteries with a VSP2 adiabatic calorimeter, J. Hazard. Mater. 192 (2012) 99–107.
[17] W.C. Chen, Y.W. Wang, C.M. Shu, Adiabatic calorimetry test of the reaction kinetics and self-heating model for 18650 Li-ion cells in various states of charge, J. Power Sources 318 (2016) 200–209.
[18] G.G. Botte, T.J. Bauer, MRSST a new method to evaluate thermal stability of electrolytes for lithium ion batteries, J. Power Sources 119-121 (2003) 815–820.
[19] Y.S. Duh, C.Y. Lee, Y.L. Chen, C.S. Kao, Characterization on the exothermic behaviors of cathode materials reacted with ethylene carbonate in lithium-ion battery studied by differential scanning calorimeter (DSC), Thermochim. Acta 642 (2016) 88–94.
[20] Y. Furushima, C. Yanagisawa, T. Nakagawa, Y. Aoki, N. Muraki, Thermal stability and kinetics of delithiated $LiCoO_2$, J. Power Sources 196 (2011) 2260–2263.
[21] Q. Wang, P. Ping, J. Sun, C. Chen, The effect of mass ratio of electrolyte and electrodes on the thermal stabilities of electrodes used in lithium ion battery, Thermochim. Acta 517 (2014) 16–23.
[22] P. Ping, Q. Wang, P. Huang, J. Sun, C. Chen, Thermal behavior analysis of lithium-ion battery at elevated temperature using deconvolution method, Applied Energy 129 (2014) 261–273.
[23] X. Liu, Z. Wu, S.I. Stoliarov, M. Denlinger, A. Masias, K. Snyder, Heat release during thermally-induced failure of a lithium-ion battery: Impact of cathode decomposition, Fire Safety J. 85 (2016) 10–22.
[24] Y. Fu, S. Lu, K. Li, C. Liu, X. Cheng, H. Zhang, An experimental study on burning behaviors of 18650 lithium ion batteries using a cone calometer, J. Power Sources 273 (2015) 216–222.
[25] T.D. Hatchard, D.D. MacNeil, A. Basu, J.R. Dahn, Thermal model of cylindrical and prismatic lithium-ion cells, J. Electrochem. Soc. 148 (2001) A755–A761.
[26] R. Spotnitz, J. Franklin, Abuse behavior of high-power, lithium-ion cells, J. Power Sources 113 (2003) 81–100.
[27] G.H. Kim, A. Pesaran, R. Spotnitz, A three-dimensional thermal abuse model for lithium-ion cells, J. Power Sources 170 (2007) 476–489.
[28] C.F. Lopez, J.A. Jeevarajan, P.P. Mukherjee, Characterization of lithium-ion battery thermal abuse behavior using experimental and computational analysis, J. Electrochem. Soc. 162 (10) (2015) A2163–A2173.
[29] P. Peng, F. Jiang, Thermal safety lithium-ion batteries with various cathode materials: A numerical study, Int. J. Heat Mass Trans. 103 (2016) 1008–1016.
[30] P.T. Coman, S. Rayman, R.E. White, A lump model of venting during thermal runaway in a cylindrical lithium cobalt oxide lithium-ion cell, J. Power Sources 307 (2016) 56–62.
[31] A. Melcher, C. Ziebert, M. Rohde, H.J. Seifert, Modeling and simulation of the thermal runaway behavior of cylindrical Li-ion cells-computing of critical parameters, Energies 9 (2016) 292–310.
[32] S. Abada, G. Marlair, A. Lecocq, M. Petit, V. Sauvant-Moynot, F. Huet, Safety focused modeling of lithium-ion batteries: A review, J. Power Sources 306 (2016) 178–192.
[33] P. Ping, D. Kong, J. Zhang, R. Wen, J. Wen, Characterization of behaviour and hazards of fire and deflagration for highenergy Li-ion cells by over-heating, J. Power Sources 398 (2018) 55–66.
[34] D. Ren, X. Liu, X. Feng, L. Lu, M. Ouyang, J. Li, X. He, Model-based thermal runaway prediction of lithium-ion batteries from kinetic analysis of cell components, Applied Energy 228 (2018) 633–644.
[35] X. Feng, C. Weng, M. Ouyang, J. Sun, Online internal short circuit detection for a large format lithium ion battery, Applied Energy 161 (2016) 168–180.
[36] A.H. Lee, S.J. Bae, M. Jang, A study on effect of lithium ion battery design variables upon features of thermal-runaway using mathematical model and simulation, J. Power Sources 293 (2015) 498–510.
[37] D Ren, X Feng, L Lu, M Ouyang, S Zheng, J Li, X He, An electrochemical-thermal coupled overcharge-to-thermal-runaway model for lithium ion battery, J. Power Sources 364 (2017) 328–340.
[38] T. Gao, Z. Wang, S. Chen, L. Guo, Hazardous characteristics of charge and discharge of lithium-ion batteries under adiabatic environment and hot environment, Int. J. Heat Mass Trans. 141 (2019) 419–431.
[39] F. Jiang, K. Liu, Z. Wang, X. Tong, L. Guo, Theoretical analysis of lithium-ion battery's failure characteristics under different states of charge, Fire and Materials 42 (2018) 680–686.
[40] X. Feng, S. Zheng, D. Ren, X. He, L. Wang, H. Cui, X. Liu, C. Jin, F. Zhang, C. Xu, H. Hsu, S. Gao, T. Chen, Y. Li, T. Wang, H. Wang, M. Li, M. Ouyang, Investigating the thermal runaway mechanisms of lithium-ion batteries based on thermal analysis database, Applied Energy 246 (2019) 53–64.
[41] X. Feng, X. He, M. Ouyang, L. Wang, L. Lu, D. Ren, S. Santhanagopalan, A coupled electrochemical-thermal failure model for predicting the thermal runaway behavior of lithium-ion batteries, J. Electrochem. Soc. 165 (16) (2018) A3748–A3765.
[42] R.E. Lyon, R.N. Walters, Energetics of lithium ion battery failure, J. Hazard. Mater. 318 (2016) 164–172.
[43] X. Feng, M. Fang, X. He, M. Ouyang, L. Lu, H. Wang, M. Zhang, Thermal runaway features of large format prismatic lithium-ion battery using extended volume accelerating rate calorimetry, J. Power Sources 255 (2014) 294–301.
[44] A.W. Golubkov, D. Fuchs, J. Wagner, H. Wiltsche, C. Stangl, G. Fauler, G. Voitic, A. Thaler, V. Hacker, Thermal runaway experiments on consumer Li-ion batteries with metal-oxide and olivin-type cathodes, RSC Adv. 4 (2014) 3633–3642.
[45] X. Feng, S. Zheng, X. He, L. Wang, Y. Wang, D. Ren, M. Ouyang, Time sequence map for interpreting the thermal runaway mechanism of lithium-ion batteries with $LiNi_xCo_yMn_zO_2$ cathode, Front. Energy Res. 6 (2018) 1–16.
[46] J. Yamaki, Y. Shinjo, T. Doi, S. Okada, The rate equation for oxygen evolution by decomposition of LixCoO2 at elevated temperatures, J. Electrochem. Soc. 161 (10) (2014) A1648–A1654.
[47] V. Yurkiv, S. Sharifi-Asl, A. Ramasubramanian, R. Shahbazian-Yassar, F. Mashayek, Oxygen evolution and phase transformation in LCO cathode: A phase-field modeling study, Comp. Mater. Sci. 140 (2017) 299–306.
[48] A. Khawam, D.R. Flanagan, Solid-state kinetics models: Basics and Mathematical fundamentals, J. Phys. Chem. B 110 (2006) 17315–17328.
[49] S. Vyazokin, C.A. Wight, Kinetics in solid, Annu. Rev. Phys. Chem. 48 (1997) 125–149.
[50] Y.S. Duh, M.T. Tsai, C.S. Kao, Characeterization on the thermal runaway of commercial 18650 lithium-ion batteries used in electric vehicle, J. Therm. Anal. Calorim. 127 (1) (2017) 983–993.
[51] Y.S. Duh, M.T. Tsai, C.S. Kao, Thermal runaway on 18650 lithium-ion batteries containing cathode materials with and without the coating of self-terminated oligomers with hyper-branched architecture (STOBA) used in electric vehicles, J. Therm. Anal. Calorim. 129 (2017) 1935–1948.
[52] B. Lei, W. Zhao, C. Ziebert, N. Uhlmann, M. Rohde, H.J. Seifert, Experimental analysis of thermal runaway in 18650 cylindrical Li-ion cells using an accelerating rate calorimeter, Batteries 3 (2017) 1–14.
[53] A.W. Golubkov, S. Scheikl, P. Planteu, G. Voitic, H. Wiltsche, C. Stangl, G. Fauler, A. Thaler, V. Hacker, Thermal runaway of commercial 18650 Li-ion batteries with LFP and NCA cathodes-impact of charge and overcharge, RSC Adv. 5 (2015) 57171–57186.
[54] F. Larsson, B.E. Mellander, Abuse by external heating, overcharge and short circuiting of commercial lithium-ion battery cells, J. Electrochem. Soc. 161 (2014) A1611–A1617.
[55] P. Röder, B. Stiaszny, J.C. Ziegler, N. Baba, P. Lagaly, H.D. Wiemhofer, The impact of calendar aging on the thermal stability of a $LiMn_2O_4$-$Li(Ni_{1/3}Mn_{1/3}Co_{1/3})$ O_2/graphite lithium-ion cell, J. Power Sources 268 (2014) 315–325.
[56] P.T. Coman, E.C. Darcy, C.T. Veje, R.E. White, Modelling Li-ion cell thermal runaway triggered by an internal short device using an efficiency factor and Arrhenius formulations, J. Electrochem. Soc. 164 (4) (2017) A587–A593.
[57] M. Parhizi, M.B. Ahmed, A. Jain, Determination of the core temperature of a Li-ion cell during thermal runaway, J. Power Sources 370 (2017) 27–35.
[58] R. Venkatachalapathy, C.W. Lee, W. Lu, J. Prakash, Thermal investigations of transition metal oxide cathodes in Li-ion cells, Electrochem. Commun. 2 (2000) 104–107.
[59] ASTM E2781-16, Standard Practice for Evaluation of Methods for Determination of Kinetic Parameters by Thermal Analysis.
[60] M.E. Brown, M. Mciejewski, S. Vyazovkin, R. Nomen, J. Sempere, A. Burnham, J. Opfermann, R. Srrey, H.L. Anderson, A. Kemmler, R. Keuleers, J.J. Hanssens, H.O. Desseyn, C.R. Lee, T.B. Tang, B. Roduit, J. Malek, T. Mitsuhashi, Computational aspects of kinetic analysis Part A: The ICTAC kinetics project-Data, methods and results, Thermochim. Acta 355 (2000) 125–143.
[61] D. Bernardi, E. Pawlikowski, J. Newman, A general energy balance for battery systems, J. Electrochem. Soc. 132 (1985) 5–12.
[62] D. Doyle, T.F. Fuller, J. Newman, Modeling of a galvanostatic charge and discharge of the lithium/polymer/insertion cell, J. Electrochem. Soc. 140 (1993) 1526–1533.
[63] J. Newman, K.E. Thomas, H. Hafezi, D.R. Wheeler, Modeling of lithium-ion batteries, J. Power Sources 119–121 (2003) 838–843.
[64] D.P. Finegan, J.J. Darst, W.Q. Walker, Q. Li, C. Yang, R. Jervis, T.M.M. Heenan, J. Hack, J.C. Thomas, A. Rack, D.J.L. Brett, P.R. Shearing, M. Keyser, E.C. Darcy, Modelling and experiments to identify high-risk failure scenarios for testing the safety of lithium-ion cells, J. Power Sources 417 (2019) 29–41.
[65] S. Santhanagoplan, P. Ramadass, J.(Zhengming) Zhang, Analysis of internal short-circuit in a lithium ion cell, J. Power Sources 194 (2009) 550–557.
[66] J. Xu, Y. Wu, S. Yin, Investigation of effects of design parameters on the internal short-circuit in cylindrical lithium-ion batteries, RSC Adv. 7 (2017) 14360–14371.
[67] X. Liu, D. Ren, H. Hsu, X. Feng, G.L. Xu, M. Zhuang, H. Gao, L. Lu, X. Han, Z. Chu, J. Li, X. He, K. Amine, M. Ouyang, Thermal runaway of lithium-ion batteries without internal short circuit, Joule 2 (2018) 1–18.
[68] X.M. Feng, X.P. Ai, H.X. Yang, A positive-temperature-coefficient electrode with thermal cut-off mechanism for use in rechargeable lithium batteries, Electrochem. Commun. 6 (2004) 1021–1024.
[69] T.H. Dubaniewicz Jr., J.P. DuCarme, Are lithium ion cells intrinsically safe? IEEE Trans. On Ind. Appl. 49 (6) (2013) 2451–2460.
[70] ASTM E2041-18, Standard test method for estimating kinetic parameters by differential scanning calorimeter using the Borchardt and Daniels method.
[71] ASTM E698-18, Standard Test Method for Arrhenius Kinetic Constants for Thermally Unstable Materials Using Differential Scanning Calorimetry and the Flynn/Wall/Ozawa Method.

[72] ASTM E2890-18, Standard test method for estimating kinetic parameters for thermally unstable materials by differential scanning calorimeter using the Kissinger method.
[73] H.J. Borchardt, H. Daniels, The application of differential thermal analysis to the study of reaction kinetics, J. Am. Chem. Soc. 79 (1957) 41–46.
[74] H.L. Friedman, Kinetics of thermal degradation of char-forming plastics from thermo-gravimetry, Application to a phenolic plastic, J. Poly. Sci. C 50 (1965) 183–195.
[75] J.H. Flynn, L.A. Wall, General treatment of the thermogravimetry of polymers, J. Res. Natl. Bur. Stand. Sect A 70 (1966) 487–523.
[76] T. Ozawa, A new method analyzing thermogravimetric data, Bull. Chem. Soc. Jpn. 38 (1965) 1881–1886.
[77] T. Ozawa, Thermal analysis-review and prospect, Thermochim. Acta 355 (2000) 35–42.
[78] H.E. Kissinger, Reaction kinetics in differential thermal analysis, Anal. Chem. 29 (1957) 109–117.
[79] *Advanced Kinetics and Technology Solutions*, AG, Switzerland.
[80] *Thermal safety software. Cheminform*St. Petersburg Ltd., St. Petersburg, Russian.
[81] D.I. Twonsend, J.C. Tou, Thermal hazard evaluation by an accelerating rate calorimeter, Thermochim. Acta 37 (1980) 1–30.
[82] ASTM E1981-12, Standard Guide for Assessing Thermal Stability of Materials by Methods of Accelerating Rate Calorimetry.
[83] S. Zhang, M.S. Ding, K. Xu, J. Allen, T.R. Jow, Understanding solid electrolyte interface film formation on graphite electrodes, Electrochem. Solid St. Lett. 4 (12) (2001) A206–A208.
[84] D.D. MacNeil, D. Larcher, J.R. Dahn, Comparison of the reactivity of various carbon electrode materials with electrolyte at elevated temperature, J. Electrochem. Soc. 146 (10) (1999) 3596–3602.
[85] Z. Chen, Y. Qin, Y. Ren, W. Lu, C. Orendorff, E.P. Roth, K. Amine, Multi-scale study of thermal stability of lithiated graphite, Energy Environ. Sci 4 (2011) 4023–4030.
[86] H. Yang, H. Bang, K. Amine, J. Prakash, Investigations of the exothermic reactions of natural graphite anode for Li-ion batteries during thermal runaway, J. Electrochem. Soc. 152 (2005) A73–A79.
[87] W.J. Ou, Y.S. Duh, C.S. Kao, J.M. Hsu, Thermal instabilities of organic carbonates with discharged cathode materials in lithium-ion batteries, J. Therm. Anal. Calorim. 116 (2014) 1111–1116.
[88] Y.S. Duh, W.J. Ou, C.S. Kao, J.M. Hsu, Thermal Instabilities of Organic Carbonates with Charged Cathode Materials in Lithium-ion Batteries, J. Therm. Anal. Calorim. 116 (2014) 1105–1110.
[89] D.D. MacNeil, J.R. Dahn, The reaction of charged cathodes with nonaqueous solvents and electrolytes: I. $Li_{0.5}CoO_2$, J. Electrochem. Soc. 148 (2001) 1205–1210.
[90] Y. Baba, S. Okada, J. Yamaki, Thermal stability of Li_xCoO_2 cathode for lithium ion battery, Solid State Ionics 148 (2002) 311–316.
[91] Q. Wang, J. Sun, C. Chen, X. Zhou, Thermal properties and kinetics study of charged $LiCoO_2$ by TG and C80 methods, J. Therm. Anal. Calorim. 92 (2) (2008) 563–566.
[92] Q. Wang, J. Sun, X. Chen, G. Chu, C. Chen, Effects of solvents and salt on the thermal stability of charged $LiCoO_2$, Mater. Res. Bull. 44 (2009) 543–548.
[93] C.Y. Jhu, Y.W. Wang, C.Y. Wen, C.M. Shu, Thermal runaway potential of $LiCoO_2$ and $Li(NiCoMn)O_2$ batteries determined with adiabatic calorimetry methodology, Applied Energy 100 (2012) 127–131.
[94] H.U. Escobar-Hernandez, M. Sam Mannan, Thermal runaway in lithium-ion batteries: Incidents, Kinetics of the runaway and assessment of factors affecting its initiation, J. Electrochem. Soc. 163 (13) (2016) A2691–A2701.
[95] M.G. Evans, M. Polanyi, Inertia and Driving Force of Chemical Reactions, Trans. Faraday Soc. 34 (1) (1938) 11–24.
[96] B.P. Roberts, J.A.J. Steel, An extended form of the Evans-Polanyi equation: a simple empirical relationship for the prediction of activation energies for hydrogen-atom transfer reactions, J. Chem. Soc. Perkin Trans. 2 (1994) 2155–2162.
[97] S. Zeman, The relationship between the kinetic data of the low-temperature thermolysis and the heat of explosion of inorganic azides, Thermochim. Acta 80 (1984) 137–141.
[98] S. Zeman, New application of kinetic data of the low-temperature thermolysis and the heat of explosion of nitroparaffins, Thermochim. Acta 261 (1995) 195–207.
[99] S.R. Saraf, W.J. Rogers, M. Sam Mannan, Application of transition state theory for thermal stability prediction, Ind. Eng. Chem. Res. 42 (2003) 1341–1346.
[100] M. Maciejewski, A. Reller, How (un)reliable are kinetic data of reversible solid-state decomposition processes? Thermochim. Acta 110 (1987) 145–152.
[101] Y.S. Duh, C.S. Kao, W.L.W. Lee, Chemical kinetics on thermal decompositions of dicumyl peroxide studied by calorimetry: An overview, J. Therm. Anal. Calorim. 127 (1) (2017) 1089–1098.
[102] Y.S. Duh, C.S. Kao, W.L.W. Lee, Chemical kinetics on thermal decompositions of di-tert-butyl peroxide studied by calorimetry: An overview, J. Therm. Anal. Calorim. 127 (1) (2017) 1071–1087.
[103] Y.S. Duh, J.M. Yo, W.L. Lee, C.S. Kao, J.M. Hsu, Thermal Decompositions of Dialkyl Peroxides Studied by DSC, J. Therm. Anal. Calorim. 118 (2014) 339–347.
[104] M. Fleichhammer, T. Waldman, G. Bisle, B. Hogg, M. Wohlfahrt-Mehrens, Interaction of cycle aging at high-rate and low temperatures and safety in lithium-ion batteries, J. Power Sources 274 (2015) 432–439.
[105] H. Ishikawa, O. Mendoza, Y. Sone, M. Umeda, Study of thermal deterioration of lithium-ion secondary cell using an accelerated rate calorimeter (ARC) and AC impedance method, J. Power Sources 198 (2012) 236–242.
[106] J.B. Zeldowitsch (Ed.), Frank-Kamenetzki D.A., A Theory of Thermal Propagation of Flame, pp.131-140 in Dynamics of Curved Fronts, Edited ByPierre Pelcé, Academic Press. Inc, 1998.
[107] M. Holzapfel, F. Alloin, R. Yazami, Calorimetric investigation of the reactivity of the passivation film on lithiated graphite at elevated temperatures, Electrochim. Acta 49 (2004) 581–589.
[108] K. Xu, Nonaqueous liquid electrolytes for lithium-based rechargeable batteries, Chem. Rev. 104 (2004) 4303–4417.
[109] K. Mukai, T. Inoue, M. Hasegawa, Rationalizing thermal reactions of C_6Li_x negative electrode with nonaqueous electrolyte, J. Power Sources 366 (2017) 185–192.
[110] A. Veluchamy, C.H. Doh, D.H. Kim, J.H. Lee, H.M. Shin, B.S. Jin, H.S. Kim, S.I. Moon, Thermal analysis of Li_xCoO_2 cathode material of lithium-ion battery, J. Power Sources 189 (2009) 855–858.
[111] G.H. Kim, K. Smith, A. Pesaran, Lithium-ion battery safety study using multi-physics internal short-circuit model, The 5-th International Symposium on Large Lithium-ion Battery Technology and Application in Conjunction with AABC09, June 9-19, Long Beach, CA, USA, 2009.
[112] J. Šesták, G. Berggren, Study of the kinetics of the mechanism of solid-state reaction at increasing temperature, Thermochim. Acta 3 (1971) 1–12.
[113] S. Yayashi, W. Walker, D. Doughty, H. Ardebili, Energy distributions exhibited during thermal runaway of commercial lithium ion batteries used for human spaceflight applications, J. Power Sources 329 (2016) 197–206.
[114] R.K. Agrawal, On the compensation effect, J. Them. Anal. Calorim. 31 (1986) 73–86.
[115] A. Mianowski, R. Bigda, The Kissinger law and isokinetic effect Part I. Most common solutions of thermokineic equations, J. Them. Anal. Calorim. 74 (2003) 953–973.
[116] A. Mianowski, R. Bigda, The Kissinger law and isokinetic effect Part II. Experimental analysis, J. Them. Anal. Calorim. 75 (2004) 355–372.
[117] M.E. Brown, A.K. Galwey, The significance of “Compensation effects” appearing in data published in ”Computational aspects of kinetic analysis”: ICTAC project, 2000, Thermochim. Acta 387 (2002) 173–183.